# Resonant Interaction of Energetic Ions with Alfvén-like Perturbations in Stellarators

N. KARULIN, H. WOBIG

IPP 2/326 April 1994


MAX-PLANCK-INSTITUT FÜR PLASMAPHYSIK

85748 GARCHING BEI MÜNCHEN

MAX-PLANCK-INSTITUT FÜR PLASMAPHYSIK

GARCHING BEI MÜNCHEN

# Resonant Interaction of Energetic Ions with Alfvén-like Perturbations in Stellarators

N. KARULIN, H. WOBIG

IPP 2/326 April 1994

*Die nachstehende Arbeit wurde im Rahmen des Vertrages zwischen dem Max-Planck-Institut für Plasmaphysik und der Europäischen Atomgemeinschaft über die Zusammenarbeit auf dem Gebiete der Plasmaphysik durchgeführt.*

# Resonant interaction of energetic ions with Alfvén-like perturbations in stellarators

N. Karulin*, H. Wobig

Max-Planck-Institut für Plasmaphysik,
Garching bei München, FRG

**Abstract**

**The modification of passing guiding center orbits of 3.5 MeV alpha particles and 45 keV protons in the presence of global Alfvén eigenmodes (GAE's) is studied in modular advanced stellarators. It is found that if resonances between particles and waves occur, drift surfaces form a set of island structures. The mode numbers of the perturbations, which are dangerous for the energetic particle confinement, are discussed for two particular stellarators (Helias reactor and Wendelstein 7-AS). The perturbation amplitudes corresponding to the onset of orbit stochasticity are studied numerically. The coefficient of the collisionless stochastic diffusion is estimated using the island width derived analytically.**

*Permanent address: Scientific Center "Kurchatov Institute", Moscow, Russia

## Introduction

The confinement of fusion alpha particles and NBI ions in toroidal systems with magnetic confinement is a crucial issue on the way to a thermonuclear reactor. The 3.5 MeV alphas provide for the self-sustaining thermonuclear reactions in plasma and the energetic NBI ions serve as one of the tools for plasma heating and non-inductive current drive in tokamaks.

Confinement properties of the both tokamak and stellarator configurations regarding the energetic particles were investigated since the early '70s by many authors. At the beginning of '80s it was realized that small rippling due to finite number of toroidal field coils in tokamaks can cause stochastization of the fast particle orbits and, consequently, the enhanced particle transport. This topic was in detail investigated during the following decade.

Another source of disturbing the magnetic field is plasma MHD activity. Last time the attention was attracted to the Alfvén eigenmodes being observed in the tokamak and, recently, stellarator plasmas. These modes can be generated by the super-thermal thermonuclear alpha particles in a reactor and by the NBI ions as well in modern machines. Exciting this instability the particles themselves interact with the perturbed by the modes magnetic field. Experimental observations carried out on tokamaks [1, 2] have shown that the essential fraction of the NBI ions can be expelled from the plasma due to TAE modes. The experiments on the stellarator Wendelstein-7AS [3] have not demonstrated, however, any enhancement of the fast ion losses in the presence of the Alfvén-like perturbations. The theory of the stochastic transport of the MeV passing ions induced by the magnetic perturbations of the Alfvén-type was recently developed [4] for tokamaks. Numerically this problem was investigated in Ref. [5].

The purpose of the present work is to analyze the influence of the Alfvén eigenmodes on the fast particle orbits in the particular stellarator configuration.

The conditions of arising of the magnetic perturbations themselves are outside of the scope of this work. It is supposed that the waves are exist as unchangeable by the particle-wave interaction background.

The paper is structured as follows: in Sec. 1 the Hamilton's equation of the parti-

cle movement are derived; the model for the stellarator magnetic field is represented in Sec. 2; the main types of the particle orbits are briefly discussed in Sec. 3; on the base of the local condition for the resonance interaction particle-wave the resonant mode numbers of the perturbation are found in Sec. 4; Sec. 5 deals with the resonant particle orbits in the Helias reactor and Sec. 6 with that of Wendelstein-7AS; the islands width and the characteristic time of the motion around the island are calculated in Sec. 7 and the results are summarized and discussed in Sec. 8.

## 1 Equations of motion

We use the guiding center equations of particle motion, since the frequencies of the magnetic field perturbation induced by the Alfvén modes are lower, than the cyclotron frequency.

The cyclic frequency of an Alfvén wave in a toroidal system can be expressed as $\omega = k_{\|} v_A$, where $v_A$ is the Alfvén velocity $v_A = B/\sqrt{4\pi n m_i}$ and $k_{\|}$ is the parallel to the magnetic field wave vector, $k_{\|} = (\mathbf{k}\cdot\mathbf{B})/B$. This frequency is much lower, than the ion cyclotron frequency $\omega_c = ZeB/mc$, what provides applicability of the guiding center approach for the investigating of the particle-wave interaction.

To derive the Hamilton's equations of motion we start with the guiding center Lagrangian [6]:

$$L(\mathbf{x},\dot{\mathbf{x}},t) = \frac{1}{2} m\, u(\mathbf{x},\dot{\mathbf{x}},t)^2 + \frac{e}{c}\,\dot{\mathbf{x}}\cdot\mathbf{A}(\mathbf{x},t) - e\,\Phi(\mathbf{x},t) - \mu B(\mathbf{x},t), \qquad (1)$$

where $\mathbf{x}$ is the position of the guiding center, $\dot{\mathbf{x}}$ is its velocity, $u$ is the parallel to the magnetic field particle velocity $u = (\mathbf{B}\cdot\dot{\mathbf{x}})/B$, $\mathbf{A}$ is the vector potential, $\Phi$ is the potential of the plasma electric field. Further, we assume the particle magnetic moment $\mu = mv_{\perp}^2/2B$ to be conserved, where $B$ denotes the magnetic field strength in the plasma.

The Lagrangian (1) describes the motion of the guiding center including the mirror force and all the conventional perpendicular drifts. Now, we construct a Hamilton's function defining, first, the momenta:

$$\mathbf{p} = \frac{\partial L}{\partial \dot{\mathbf{x}}} = mu\,\frac{\mathbf{B}}{B} + \frac{e}{c}\,\mathbf{A}.$$

The guiding center Hamiltonian immediately follows:

$$H(\mathbf{p},\mathbf{x},t) = p_i \frac{dx^i}{dt} - L(\mathbf{x},\dot{\mathbf{x}},t) = \frac{1}{2}\, mu(\mathbf{p},\mathbf{x},t)^2 + \mu B(\mathbf{x},t) + e\,\Phi(\mathbf{x},t) \qquad (2)$$

We use in this paper the so-called canonical coordinates [7] $r$, $\tilde{\theta}$, $\varphi$, in which the radial components of the magnetic field $B_r$ and vector potential $A_r$ are equal to zero. This set of coordinates differs from the usual toroidal one only in determination of the poloidal variable $\tilde{\theta}$. The last deviates from the poloidal angle $\theta$ by a quantity of order $B_r/B$. When the flux surfaces exist, the canonical coordinates are a special case of flux coordinates. Since the coordinate transformation preserves toroidal topology and the angle variable $\tilde{\theta}$ is periodic in the angles, one can express the perturbation of the vector potential induced by the Alfvén wave in the usual way:

$$\tilde{A}_{\|} = A_m(\psi)\, \cos(-n\varphi + m\theta - \omega t), \qquad (3)$$

where $m$, $n$ are respectively the poloidal and toroidal mode numbers of the wave and this potential has the sole component parallel to the magnetic field. The tilde of the poloidal variable $\tilde{\theta}$ is dropped in the following.

In the canonical coordinates used the radial component $p_r \equiv 0$, then the remaining components are:

$$\begin{aligned} p_\theta &= mub_\theta + \frac{e}{c}\,(A_\theta + \tilde{A}_{\|} b_\theta) \\ p_\varphi &= mub_\varphi + \frac{e}{c}\,(A_\varphi + \tilde{A}_{\|} b_\varphi), \end{aligned} \qquad (4)$$

where $b_{\theta,\varphi}$ are the components of the unit vector $\mathbf{b} = \mathbf{B}/B$; $A_{\theta,\varphi}$ are the components of the unperturbed vector potential and the perturbation itself is introduced through $\tilde{A}_{\|}$. We notice that if $\tilde{A}_{\|}$ is normalized such that

$$\tilde{\alpha} \equiv \frac{\tilde{A}_{\|}}{BR},$$

than the perturbing magnetic field induced by the wave can be determined as following [8]:

$$\delta\mathbf{B} = \nabla \times \tilde{\alpha}\mathbf{B},$$

thus $\tilde{\alpha}$ is a scale factor to $\delta\mathbf{B}$.

Experimentally measured variations of the magnetic field caused by the Alfvén-like MHD activity do not exceed the value $\delta B/B \sim 10^{-4}$. That is why $\tilde{\alpha}$ is a small

parameter allowing us to reduce the above equations (4). Comparing the terms in the first of them, it is seen that the perturbation $\tilde{A}_{\|} b_\theta$ can be neglected being smaller by a factor $\tilde{\alpha} \iota/2$ than the term $A_\theta$. The first term $mub_\theta$ relates to the second one as $2\rho_{\|}/R$ and can be also dropped in our case.

Thus, the momenta (4) take the following form:

$$\begin{aligned} p_\theta &= \frac{e}{c} A_\theta \\ p_\varphi &= mub_\varphi + \frac{e}{c}(A_\varphi + \tilde{A}_{\|} b_\varphi), \end{aligned} \tag{5}$$

To invert these equations in order to obtain the parallel velocity as a function of the momenta and coordinates it is needed to exclude the components of the unperturbed vector potential $A_{\theta,\varphi}$. For this sake we use, first, the rotational transform $\iota$ defined as

$$\iota = \frac{d\zeta}{d\psi} = -\frac{dA_\varphi}{dA_\theta},$$

where $\zeta$ is the poloidal and $\psi$ is the toroidal magnetic flux. The sign minus is explained by the fact that the coordinate system used is left-handed. Since the vector potential is the function of the magnetic surface, the last equation can be resolved,

$$A_\varphi = -\iota A_\theta + \int^{\psi} \iota' A_\theta \, d\psi,$$

where $\iota' = d\iota/d\psi$.

Now, substituting the first equation (5) into the second one and excluding $A_\varphi$ one obtains $p_\varphi$ :

$$p_\varphi = mub_\varphi - \iota p_\theta + \int^{\psi} \iota' p_\theta \, d\psi + \frac{e}{c} \tilde{A}_{\|} b_\varphi,$$

and, after inverting, the required expression for the parallel velocity:

$$u = \frac{p_\varphi + \iota p_\theta - \int^{\psi} \iota' p_\theta \, d\psi - (e/c)\, \tilde{A}_{\|} b_\varphi}{mb_\varphi}.$$

If we substitute this expression into the Hamilton's function (2), we obtain the required Hamiltonian $H(p_\theta, p_\varphi, \psi, \theta, \varphi, t)$. To reduce the number of variables to two pairs we notice that the flux $\psi$ can be replaced in principle by $p_\theta$ with the help of the first equation (5). Namely,

$$\oint_C A_\theta d\theta = 2\pi A_\theta(\psi) = \iint \mathbf{B}\, d\mathbf{S} = B_0 \pi < r >^2,$$

where $C$ is the contour $\theta = const$ lying on the magnetic surface, $<r>$ is the average radius of this magnetic surface and $B_0$ is the magnetic field on the axis. Taking into account that the plasma electric potential is constant on a magnetic surface $\Phi = \Phi(\psi(<r>))$, we rewrite the guiding center Hamiltonian in the final form:

$$H(p_\theta, p_\varphi, \theta, \varphi, t) = \frac{1}{2mb_\varphi^2}\left(p_\varphi + \iota p_\theta - \int^r \iota' p_\theta \, dr - \frac{e}{c}\tilde{A}_\parallel b_\varphi\right)^2 + \mu B(p_\theta, \theta, \varphi) + e\,\Phi(p_\theta).$$

We have dropped $<r>$ and replaced it with $r$ keeping in mind that it is not a real radius but some averaged one. Dealing with the configurations with the large aspect ratio $R/a \sim 10$, we take $b_\varphi = B_\varphi/B$ equal to the major radius of the torus $R$.

The dependencies $\iota(r)$, $B(r, \theta, \varphi)$ and $\Phi(r)$, where

$$r^2 = \frac{2c}{eB_0} p_\theta,$$

characterize the particular magnetic configuration and, being specified, together with $\tilde{A}_\parallel$ fully describe the problem considered.

Finally, we write out explicitly the equations of motion of a single particle:

$$\begin{aligned}
\dot{p_\theta} &= \frac{e}{mcR}\left(p_\varphi + \iota p_\theta - \int^r \iota' p_\theta \, dr - \frac{e}{c}\tilde{A}_\parallel R\right)\frac{\partial \tilde{A}_\parallel}{\partial \theta} - \mu\frac{\partial B}{\partial \theta} \\
\dot{p_\varphi} &= \frac{e}{mcR}\left(p_\varphi + \iota p_\theta - \int^r \iota' p_\theta \, dr - \frac{e}{c}\tilde{A}_\parallel R\right)\frac{\partial \tilde{A}_\parallel}{\partial \varphi} - \mu\frac{\partial B}{\partial \varphi} \qquad (6) \\
\dot{\theta} &= \frac{1}{mR^2}\left(p_\varphi + \iota p_\theta - \int^r \iota' p_\theta \, dr - \frac{e}{c}\tilde{A}_\parallel R\right)\left(\iota - \frac{eR}{c}\frac{\partial \tilde{A}_\parallel}{\partial p_\theta}\right) + \mu\frac{\partial B}{\partial p_\theta} + e\frac{\partial \Phi}{\partial p_\theta} \\
\dot{\varphi} &= \frac{1}{mR^2}\left(p_\varphi + \iota p_\theta - \int^r \iota' p_\theta \, dr - \frac{e}{c}\tilde{A}_\parallel R\right).
\end{aligned}$$

Actually, the variable $p_\theta$ is a measure of the radial distance of the particle guiding center from the plasma axis.

## 2 Model magnetic field

Common representation of a stellarator magnetic field strength in Fourier components is

$$\frac{B}{B_0} = C_{0,0} + \sum C_{m,l}\cos(Mm\varphi)\cos(l\theta) + \sum S_{m,l}\sin(Mm\varphi)\sin(l\theta), \qquad (7)$$

where $\varphi$, $\theta$ are toroidal and poloidal angle-like coordinates, $m$, $n$ are the numbers of the Fourier harmonics and $M$ is the number of the toroidal periods (in our case $M = 5$). All the coefficients $C_{m,l}$, $S_{m,l}$ can be radially dependent.

Deriving the equations of motion (6) we have used the canonical system of coordinates, which differs from that typically used in the Fourier decomposition above. But the periodical in angles structure of the both of them makes possible to use formula (7) in canonical coordinates. It must be kept in mind that, strictly speaking, the radial profiles of the Fourier coefficients should be now recalculated for the canonical coordinates. However, the difference for the passing orbits seems not to be principle.

For the Helias configuration considered here we may retain only a few of the terms in (7) to give satisfactory model of $B$ which keeps the main features of the magnetic field. The typical set of the coefficients for the reactor case is represented in Fig. 1a [9]. Comparison of our model, containing the following non-zero coefficients: $C_{0,0}$, $C_{0,1}$, $C_{1,0}$, $C_{1,1}$ and $S_{1,1}$ with the results of the calculation of $B(\theta,\varphi)_{r=const}$ with the full set of Fourier harmonics is shown in Fig. 2.

The components $C_{1,1}$, $S_{1,1}$ describe the main helical dependence of the magnetic field strength. The modular structure of the magnetic field is represented by the term $C_{0,1}\cos(M\varphi)$ and the toroidicity by the term $C_{1,0}\cos(l\theta)$. The last two terms can cause particle trapping as well as the main helical well. The coefficient $C_{0,0} \sim 1$, which is not represented on the plot, depends only slightly on the plasma radius when plasma $\beta$ is small. At maximal achievable plasma $\beta \sim 0.04 - 0.05$, as show the equilibrium calculations, the magnetic field on the axis is reduced due to diamagnetic effect (by about 10 % of its vacuum value). This effect changes the radial dependence of the coefficient $C_{0,0}$.

Due to its simplicity the Helias configuration provides an interesting object for analysis and, moreover, some details of particle motion and the main orbit types can be understood without numerical calculations.

The magnetic configuration realized in the second case considered, namely of Wendelstein-7AS, is not so simple as the previous one. The number of Fourier harmonics contributing to the value $B$ is relatively great (s. Fig. 1b). To shorten the computer time we have curtailed the number of coefficients up to $m = 0, ..., 4$; $l = 0, ..., 2$. The radial dependent coefficients themselves were taken from the equilibrium calculations [10]. Figure 3 shows the model field strength $B$ used in our calculations

concerning NBI ions in W-7AS and the same value obtained from the equilibrium code VMEC.

Of course, the model of the magnetic field strength can be naturally extended to any number of Fourier harmonics, but that affects the required computer time.

## 3 Particle orbit types

In order better to understand the following results concerning the particle-wave interaction we briefly discuss in this section the main types of particle orbits on the example of the Helias reactor.

Since the mirror forces arising from the space inhomogeneity of the magnetic field together with the motion along the field line determine basically the particle orbits, it is helpful for the orbit analysis to use the maps of the magnetic field strength via the angle coordinates $\theta$, $\varphi$. Such a map presented in Fig. 1a should be supplemented with a field line which is straight at the constant radial label $r$.

Inside one of the field periods there are seen a well and two hills. A passing particle with $\mu = 0$ follows the field line and does not change its parallel velocity. If, however, the particle velocity has a perpendicular to the magnetic field component $v_{\|}$, the drifts force the guiding center to diverge from the field line in poloidal direction. The particles with large perpendicular velocity can be reflected from the regions with the sufficiently strong magnetic field and become trapped. In our case such deeply trapped particles can be blocked in the region adjacent to the point $\theta = \pi$, $\varphi = \pi$ ("central well").

Another sort of the orbits are those which are reflected in the region between the separatrix surrounding the central well ("first separatrix") and the next one surrounding two hills ("second separatrix"). These orbits, being trapped toroidally but not poloidally, undergo poloidal precession due to the conventional drifts which nature we do not discuss now in details.

There are also the orbits that are able to surmount the barrier of the second separatrix (actually, its field strength) but cannot pass the hill over its top. These particles are not isolated toroidally, they run over the passings from one field period to another.. Helically moving around the torus and shifting poloidally they finally

meet a region with a field strength high enough for them to be reflected. The radial width of this kind of orbits is the largest.

So, for the magnetic configuration considered, there are four main types of the particle orbits: a) pure passing orbits; b) trapped in the central well; c) toroidally trapped inside the first separatrix and d) transit or superbanana orbits.

Actually, these types do not cover the whole set of possible orbits. Under some circumstances the drifts can detrap, for example, the orbits of the type b), but this classification is useful as a first step in investigating of the particle behaviour.

## 4 Particle-wave resonances

We discuss now the resonance condition for the fast particles interacting with the Alfvén-type wave. The main purpose of the following treatment is to predict the dangerous wave mode numbers, which interact with the energetic particles, modify their orbits substantially and can lead to collisionless losses.

Since the amplitude of the magnetic field perturbation produced by the wave is much lower than the background equilibrium field, it is evident to expect that the influence of the wave on the particle orbit is the strongest in the resonance case. The resonance will be achieved locally if the following condition is satisfied:

$$\omega - k_{\|} v_{\|} - \mathbf{k}_{\perp} \mathbf{v}_d = 0, \tag{8}$$

where $\omega = k_{\|} v_A$ is the cyclic frequency of the Alfvén wave, $\mathbf{v}_d$ is the drift velocity and $k_{\|} = (m\iota - n)/R$, $k_{\perp} = m/r$ are the parallel and perpendicular components of the wave vector.

Let us consider the last equation in more details. In the absence of the drifts ($\mathbf{v}_d = 0$) the resonance condition can be satisfied only if $v_{\|} = v_A$. [1] The Alfvén velocity in the reactor is lower, than the alpha particle velocity, so that $v_A/v_\alpha \sim 0.4$ at the plasma axis. In W-7AS this relation for the 45 keV protons is opposite, namely $1 < v_A/v_p < 2$. That means that the the poloidal drifts play an important role in achieving of the particle-wave resonances.

Passing particles keep the sign of their parallel velocity unchanged, moreover, the magnitude of $v_{\|}$ itself changes along the orbit only weakly, thus one can replace the

[1] We do not consider here sidebands resonances

local velocity $v_{||}$ in equation (8) with some mean value $< v_{||} >$ . On the other hand, the orbits of the trapped particles are characterized with the periodical changing of their direction of movement and the transition from the local condition (8) to some "averaged" one is not so obvious.

Figure 4 illustrates graphically the resonance of a co-going particle with the wave with $m,\ n < 0$. It is seen that such a resonance could not be achieved if the particle did not drift poloidally.

Equation (8) can be rewritten in the following normalized form:

$$\gamma \equiv \frac{v_A}{v} = \sigma\sigma_k\sqrt{1-\mu B/E} + \frac{m}{\mid m\iota - n \mid}\frac{R}{r}\frac{v_d}{v},$$

where $\sigma = sign(\mathbf{vB})$, $\sigma_k = sign(k_{||})$ and the poloidal drift velocity $v_d$ also contains a sign. We emphasize that the resonance condition considered is not used to find the exact resonances but serves rather as a simple tool to facilitate the search for possible resonances.

The latter equation contains free parameters $\mu$, $\sigma$, $m$, $n$ and variable $r$. If the drift velocity $v_d$ is replaced by its mean value, the dependence on angle coordinates vanishes. Under these assumptions the resonance equation can be solved numerically if the drifts are specified.

We shall consider here two drifts, namely those caused by the radial gradient of the magnetic field and by the plasma electric field. The first was found [11] to be of particular importance for the alpha particle confinement in the Helias magnetic configuration.

As it is well known the $\nabla B$ drift can be defined as $v_{\nabla B} = -\mu(\nabla B \times \mathbf{B})/B^2$ [12]. In a stellarator case the magnetic field strength $B$ depends on all space coordinates $r,\ \theta,\ \varphi$. If, however, the guiding center orbit is not rational or, in other words, if the orbit covers the magnetic surface after many toroidal turns uniformly, the angle dependencies of this drift become averaged. For such orbits $< v_{\nabla B} >$ depends only on the radial coordinate $r$. Looking at the expression for the field strength (7) we see that the radial dependence of the Fourier coefficient $C_{0,0}$ is responsible for this drift. At high plasma $\beta$-s plasma diamagnetism causes magnetic field weakening in the core region of the plasma column. The equilibrium calculations give a value of about 10 % reduction in the plasma center at the maximal stable value of $\beta$. We

have modelled in our calculations the profile of $C_{0,0}(r)$ to be parabolic what is close to the equilibrium one.

Another source of the poloidal drift is the radial plasma electric field arisen from the ambipolar nature of the transport processes. The correspondent perpendicular drift velocity [12] is $v_E = -c(\nabla\Phi \times \mathbf{B})/B^2$, where electric potential $\Phi$ depends only on the radial coordinate $r$. It is difficult to measure the profiles of the electric fields experimentally, thus in predictions for a reactor one can rely only on the transport calculations with many uncertainties. It is, however, to expect that the field should be negative with the maximal amplitude of about 50-100 V/m for W-7AS.

It should be mentioned that if the magnetic field strength $B$ decreases from the edge to the center and the radial electric field is negative, the both drift velocities have the same poloidal direction.

Now, after specifying the drifts the last equation expressing the condition for the resonance interaction between a passing particle and the wave with the mode numbers $m$, $n$ can be solved numerically. The example of such solution for a reactor case and for the lowest mode numbers $m$, $n$ is presented in Fig. 5. Every point $(\tilde{\mu},\ r/a)$ of the curves corresponds to a resonance between the alpha particle starting on the radius $r$ and having the normalized magnetic moment $\tilde{\mu}$, where $\tilde{\mu} \equiv \mu B_0/E$. The dotted curve above denotes the boundary between the pure passing orbits and the majority of the trapped ones, for which the used in this section approach is not applicable.

It is seen that co– and counter-going particles resonate with the different mode numbers $m$, $n$. This result is apparent, because when the sign of $v_\parallel$ in equation (8) has been changed, the drift velocity $v_d$ does not change its sign.

We will discuss these results in detail in the next section.

## 5 Resonant particle orbits

The interaction of the passing MeV ions in tokamaks with low frequency magnetic perturbations (TAE's) was investigated recently by Mynick [4]. It was found that the drift surfaces form island-like structures if resonance occurs between the perturbation and the particle guiding center orbit. The formation of the islands in

drift surfaces having the finite radial width, can cause enhanced immediate losses of the energetic particles from the plasma, as well as can give rise to the stochastic transport.

The question arises whether such island structures exist in stellarators. The condition of the resonant interaction particle-wave cannot be fulfilled permanently by varying along the orbit magnetic field $B$ in the principally three dimensional configuration. On the other hand, the islands in the low-shear configurations typical for the both modular stellarators under consideration are expected to have greater radial extension, than in tokamaks.

To choose the orbit parameters for numerical calculation the solution of equation (8) shown in Fig. 5 was used. Although they are not exact, the curves give an idea where to search for resonances. Actually, such a picture contains a lot of information concerning particle-wave interaction. First, one can see, whether the resonances are in general expected for the given mode numbers in the given stellarator [2]. If there are no solutions of the equation (8), the resonances between the passing particle and the wave do not occur. Next, changing the plasma parameters such as density and its profile, magnetic field strength $B$ and the particle energy it is possible to optimize the configuration without carrying out of detailed analysis. Third, the influence of $\iota$-profiles on the radial distance between the neighbouring islands can be studied. Finally, an interesting effect of resonance superposition can be predicted. Crossings of the curves in Fig. 5a mean that the orbit can resonate with two modes simultaneously, i. e. the orbit parameters fulfill the resonance conditions with two modes (e. g., counter-going orbit with $\tilde{\mu} = 0.7$, $r/a = 0.6$ resonates with the modes $(m,\ n) = (-4, -3)$ and (6, 5) if they exist in the plasma).

It should be mentioned that the drift surface islands, unlike the magnetic islands, do not arise exactly on the rational magnetic surfaces. In the Helias case the rotational transform $\iota$ varies from 0.845 at the center up to 0.96 at the plasma edge (s. Fig. 7). As it is seen from Fig. 5 only few of the curves shown there fall into this interval, namely $n/m = 6/7,\ 7/8$ in Fig. 5a and $n/m = -6/-7,\ -8/-9,\ -9/-10$ in Fig. 5b. Moreover, some of the resonant mode numbers $m$, $n$ are far from the

[2] The same picture can be obtained for a tokamak

values of $\iota$.

This can be explained, if one looks at equation (8), which we rewrite in the following way:

$$\iota_s = \frac{n}{m} - \frac{R}{r}\frac{v_d}{v_{\|\alpha}} + \frac{\omega R}{m v_{\|\alpha}}, \qquad (9)$$

where $\iota_s$ is now the "resonance" rotational transform for the perturbation $m$, $n$. If the perturbation were static, $\omega = 0$, it was the ordinary case of stellarator magnetic islands located on the rational magnetic surfaces. Propagation of the perturbation and particle drifting with the velocity $v_d$ shift the resonance, and the resonance value of the rotational transform differs, sometimes substantially, from the value $\iota = n/m$.

The most sensitive to the magnetic field perturbation should be the orbits located in the phase space near the passing-trapped boundary. Although the magnetic moment of the particle is conserved, the particle can cross the boundary and become trapped due to radial drift if the island width is sufficiently large. Launching such a particle we observe now, how the orbit changes by increasing amplitude of the perturbation with the mode numbers $(m,\ n) = (-2, -1)$.

The Poincaré plot in Fig. 6a shows two big islands formed by the drift surfaces of the counter-going particle with $\tilde{\mu} = 0.84$ and the start radial coordinate $r/a = 0.65$. The island boundaries are spread, because of the dependence of the particle parallel velocity $v_{\|}$ on space coordinates, while the wave phase velocity was supposed to be constant. In the vicinity of the passing-trapped boundary (dotted line in Fig. 6) this effect is especially strong, since here the variations of the particle parallel velocity are the greatest. The perturbation amplitude was taken to be $\delta B/B = 10^{-4}$.

The same perturbation of the growing amplitude $\delta B/B = 2 \cdot 10^{-4}$ apparently pushes the passing orbit some more closer to the trapped boundary, island's edge is spreading, but the structure self is not still destroyed (Fig. 6b). If the perturbation achieves the value of $5 \cdot 10^{-4}$, it is seen (Fig. 6c) that the Poincaré plot of the particle orbit demonstrates no regularity more, the particle movement is rather stochastic. The islands are destroyed, since the particle undergoes now reflections. The orbit has become trapped, actually a superbanana one. The tips corresponding to reflections are seen in Fig. 6d.

Comparison of the resonant and non-resonant interaction of the passing alpha

particle with the wave demonstrates relatively weak influence of the non-resonant perturbation on the particle orbit. In Fig. 8a an alpha particle with $\tilde{\mu} = 0.5$ and $r/a = 0.54$ interact resonantly with a perturbation $(m,\ n) = (-5, -4)$ of the moderate amplitude $\delta B/B = 5 \cdot 10^{-5}$. One can see a chain of five ($\mid m \mid = 5$) big islands. Their boundaries are sharper, than in the previous case, since the location of the particle in the phase space is farther from the passing-trapped boundary.

If we launch the same particle in the opposite direction, i. e. the sign of the parallel velocity $v_{\parallel}$ is changed and other orbit parameters are not, it is no more the resonance. Even by much higher perturbation amplitude of $\delta B/B = 2.5 \cdot 10^{-3}$ the radial deviation of the orbit is lower, than in the resonance case before.

Another interesting effect is superposition of two resonances. As it was also mentioned earlier, the crossing of the curves in Fig. 5 mean that the same particle can be in resonance with two perturbations simultaneously, since these island structures are not separated radially. If we have two island chains separated spatially, the perturbations must be great enough to yield overlapping of the islands. In principle, in the case of intersecting of the resonance curves the only condition on the perturbation amplitudes is that the islands generally exist. By very low amplitudes in the 3-D magnetic field the island structures cannot exist as radially extended formations, since the boundary spreading becomes comparable with their widths, and they can no longer be distinguished. This intuitive criterion is not strict, rather illustrative, actually the better one is merging of the islands poloidally in Poincaré maps representation. For the transport applications the first one seems, however, to be more suitable.

The resonance superposition is represented in Fig. 9. It is chosen not the exact coincidence of the resonances (curves intersections in Fig. 5), but two adjacent ones, which can become coupled by means of orbits radial overlapping. Two narrow islands $(m,\ n) = (-2, -3)$ are produced by the perturbation of the amplitude $\delta B/B = 2 \cdot 10^{-4}$ (Fig. 9a). In the next picture (Fig. 9b) the perturbation $(m,\ n) = (-3, -4)$ with the amplitude $\delta B/B = 10^{-4}$ generates three islands. In the both cases the co-going orbit has the same parameters $\tilde{\mu} = 0.7$ and $r/a = 0.77$. If the two perturbations are superposed, one finds now no island-like structure; neither

the first, nor the second island chain can be seen. The radial width of the resulting orbit seems to be almost unchanged. The islands destruction is dependent on the phase shift between the perturbations, which changes the result not qualitative but quantitative.

We should mention that the drift surface islands are moving toroidally and poloidally, that is why to stop them on the Poincaré maps it is used a "viewpoint" moving with the particular island.

## 6 Resonant NBI-protons orbits in Wendelstein-7AS

Coherent MHD activity driven by the NBI ion population was recently observed in the stellarator Wendelstein-7AS [3]. It seems very likely that those modes are actually the global Alfvén waves. The typical fluctuation level of the magnetic field is about $\delta B/B \sim 10^{-4}$. No unusual effects concerning fast ion confinement was experimentally observed. We discuss below briefly the possibilities for the particle-wave resonances for the mentioned experimental conditions.

In the Helias reactor case the Alfvén velocity $v_A = B/\sqrt{4\pi n_i m_i}$ in the plasma core was about one half of the particle velocity $v_\alpha = \sqrt{2E/m_\alpha}$. In the outer plasma region the Alfvén velocity increases due to decreasing of the plasma density (Fig. 7b). These two values become equal somewhere near the plasma edge, that is why there the resonance curves come close together for almost all the modes (Fig. 5).

Another situation is typical for the W-7AS plasma: Everywhere in the plasma the Alfvén velocity is greater than $v_p$,[3] where $v_p$ is the NBI-proton velocity. If $v_A > v_p$ (the case of the high field $B = 2.5T$), the particle-wave resonances can occur at the mode numbers $m$, $n$ so that $m/n \simeq \iota$. To illustrate this statement we return to equation (9) for the "resonance" value of the rotational transform $\iota_s$, which can be once more rewritten taking into account that $\omega = v_A\,(m\iota - n)/R$:

$$\iota_s = \frac{n}{m} + \frac{v_d}{v_A}\,\frac{R}{r}\,\frac{1}{1 - v_{||}/v_A}.$$

Since the drift velocity $v_d$ is much smaller, than the Alfvén velocity $v_A$, the difference $\iota - n/m$ is always small except the case, where $v_{||} \sim v_A$.

[3] In this section the resonances between the full-energy component ($E = 45$ keV) and the wave are discussed

The typical values of the rotational transform in different regimes in W-7AS (2.5 T) are between 0.34 and 0.58. Hence, the lowest mode numbers of the perturbation whish are expected to resonate with the passing orbits are the following: $(m,\ n) = (-3,-1); (-2,-1); (-5,-2); (-5,-3)$. Figure 10 shows the solutions of the resonance equation (9) for different discharges [13].

If the Alfvén velocity is not very high and the rotational transform $\iota$ is somewhere in the plasma close to the lowest rational values, a set of resonances can occur in the same discharge simultaneously (Fig. 10a). By higher $v_A$ and by the rotational transform having no rational values inside the plasma, $\iota \neq n/m$, some of the resonances disappear (Fig. 10b). Figure 10c shows the case of high Alfvén velocity, when the resonances can appear only in the vicinity of the rational surfaces. The difference between the resonances of the co– and counter-going particles is small now.

In the regimes with the field strength $B = 1.25\,T$ the Alfvén velocity is lower, then on the axis $v_A$ nearly achieves $v_p$. Now, the resonances can occur in the broader range of the wave mode numbers and of the orbit parameters $\tilde{\mu}$, $r/a$ (Fig. 11). Rotational transform varies in these calculations from 0.27 up to 0.60 and all corresponding resonances are represented. Even the modes with $m = -5, -6, -7;\ n = -1$ resonate with the counter-going particles due to their drift shifting of the orbit from the field line (Fig. 11a).

The resonance occuring is very sensitive against the assumptions concerning the profiles of the rotational transform $\iota$, plasma radial electric field and the magnetic field strength $B(r)$. The last two determine particle drifts, which in turn bring the particles in resonance. To predict or to analyze experimental results concerning particle losses caused by the Alfvén modes one needs to know these plasma characteristics.

Finally, we present the Poincaré maps of some resonance particle orbits chosen according to the proposed procedure of resonance searching. Figure 12 shows the orbits corresponding to the resonances of Fig. 10a. There are seen the chains of five (Fig. 12a, $(m,\ n) = (-5,-2)$) islands for the co-going ion and of three islands (Fig. 12b, $(m,\ n) = (-3,-1)$) for the counter-going one. The last of the pictures (Fig. 12c) shows the resonance being very likely to the previous one, but located

on the outer branch of the curve in Fig. 10a. Two branches of the same resonance are explained by the non-monotonic profile of the rotational transform. In principle, the islands overlapping in this particular case would mean the sufficient condition for the orbit stochastization.

## 7 Collisionless transport

To treat the problem of fast particle collisionless transport in perturbed by the wave field it is needed to calculate the width of the drift islands. We obtain in this section on the basis of Hamilton's equations of motion a simple formula allowing to construct the diffusion coefficient.

For this sake we look once more at the first of equations (6). The last term rights is responsible for the deviation of the orbit from the magnetic surface due to poloidal inhomogeneity of the unperturbed magnetic field. It can be dropped for simplicity, then the equation looks like the following:

$$\dot{p_\theta} \simeq v_\parallel \frac{e}{c} \frac{\partial \tilde{A}_\parallel}{\partial \theta} = - \frac{eBR}{c} \tilde{\alpha}\, m\, v_\parallel \sin\eta, \qquad (10)$$

where $\eta = -n\varphi + m\theta - \omega t + \phi$ and $\phi$ is the initial mode phase. The normalized mode amplitude $\tilde{\alpha}$ was defined in Sec. 1.

For our needs we can use instead of the exact parallel velocity $v_\parallel$ its mean value

$$v_\parallel = < p_\varphi + \iota p_\theta - \int \iota' p_\theta \, dr >,$$

which is approximately constant in time for the particle located not very close to the passing-trapped boundary in phase space. The magnetic perturbation in the equation for the momentum (10) is represented through the derivative of the vector potential, which is proportional to $sin\eta$.

The unperturbed equations for the angles $\theta$ and $\varphi$ can be written out in the following way:

$$\begin{aligned} \dot{\theta} &= \left( \frac{v_\parallel}{R} - \frac{v_d}{r} \right) \iota \\ \dot{\varphi} &= \frac{v_\parallel}{R}, \end{aligned}$$

where $v_d$ is the particle drift velocity: $v_d = |\mu\, \partial B/\partial p_\theta + e\, \partial \Phi/\partial p_\theta|$.

Deriving the last equations under assumption that the right parts do not depend on time, one obtains the expression for the mode phase $\eta$:

$$\eta = (k_{\|} v_{\|} - k_{\perp} v_d - \omega) t + \phi, \tag{11}$$

where $k_{\|} = (m\iota - n)/R$ and $k_{\perp} = m/r$ are the components of the wave vector. The requirement of time independency of the right parts of the equations for $\theta$ and $\varphi$ means that the drift velocity $v_d$ varies weakly on the radial distance comparable with the orbit width.

To proceed with the equation for the momentum $p_\theta$ we expand $sin\eta$ in the vicinity of the resonance surface $r_s$:

$$\sin\eta \simeq \sin\eta_s + \cos\eta_s\, \eta_s' \delta r + \left(\eta_s'' \cos\eta_s - (\eta_s')^2 \sin\eta_s\right) \frac{(\delta r)^2}{2}.$$

The subscript "$s$" denotes the resonance drift surface, and the prime denotes differentiation over the normalized radius $r/a$.

We define the resonance according to Sec. 4 as the fulfillment of the following condition:

$$k_{\|}(r_s) v_{\|} - k_{\perp}(r_s)\, v_d(r_s) - \omega = 0\,.$$

To chose correctly the mode phase $\phi$ it should be noted that $\dot{p_\theta}$ on the resonance surface is maximal and $\dot{\theta}$ is equal to zero. We chose the mode phase $\phi = 3\pi/2$, then the sign of $\dot{p_\theta}$ is positive when $m$, $v_{\|}$ are both positive.

The equation for the momentum takes now the form:

$$\dot{p_\theta} = \frac{eBR}{c}\, \tilde{\alpha}\, m\, v_{\|} \left(1 - (\eta_s')^2 \cdot \frac{(r - r_s)^2}{2}\right).$$

After replacing of $p_\theta$ by the radial variable $r$ through the expression $r = 2c\,p_\theta/eB$, one obtains the equation containing only the radial position of the guiding center and time:

$$r\dot{r} = A\left(1 - C\,t^2\,(r - r_s)^2\right), \tag{12}$$

where $r$ is the radial coordinate normalized over the plasma size $a$, the time $t$ is normalized over the transit time $2\pi R/v$; $A \equiv 2\pi\,(v_{\|}/v)\,(\delta B/B)\,(R/a)$ and $C \equiv (2\pi m v_{\|}/v)^2\, \iota'^2/2$. The perturbation amplitude is introduced through

$$\frac{\delta B}{B} = \tilde{\alpha}\, m\, \frac{R}{a}.$$

The nonlinear equation (12) is expected to describe the evolution in time of the radial position of the guiding center if the orbit is resonant to the wave. Starting from the resonance surface the particle guiding center, firstly, moves away from it. The phase shift $\delta\eta$ increases, since the resonance condition above is satisfied only on the definite radius $r_s$. The perturbation of the magnetic field $\delta B$, diverging the particle from its unperturbed orbit, changes its spatially orientation. When the phase $\eta$ changes its value by $\pi/2$ the particle stops the movement outwards.

It is seen that by the large times the equation (12) describes the orbit not properly, since the solution approaches the resonance surface $r_s$ asymptotically, what does not happen in reality. The reason for that is the cut off of the higher terms in expanding of $sin\,\eta$.

We solve equation (12) analytically using an iterative method. By the short times the second right-hand-side term can be neglected, and the solution looks like:

$$r^2 = r_s^2 + 2\,A\,t.$$

Constructing from this expression the initially dropped term $\sim (r - r_s)^2$ one obtains the final equation:

$$r\,\dot{r} = A\,(1 - \frac{A^2 C}{r_s^2}\,t^4),$$

which can be solved analytically. The solution taken at the moment $t^* = (r_s/A\sqrt{C})^{1/2}$, when the time derivative of the radial variable $\dot{r}$ in the last equation becomes zero, gives the island half width:

$$\delta r = \frac{4 \cdot \sqrt[4]{2}}{5} \sqrt{\frac{R}{a}\,\frac{\delta B}{B}\,\frac{1}{m\dot{t}'}\,\frac{1}{r}}, \tag{13}$$

where $\delta r$ and $r$ are normalized over $a$.

This simple formula gives correct scaling and quantitative values for the island widths, what is confirmed by the numerical solution of equation (12). Computed from the whole set of Hamilton's equations (6) orbits demonstrate correspondence with the derived formula as well.

It is interesting to note that the expression for the island half width obtained in a different way by Mynick [4]:

$$\delta r = 2\sqrt{G_l\,\frac{R}{a}\,\frac{\delta B}{B}\,\frac{\dot{t}}{\dot{t}'}\,\frac{1}{n}},$$

where $G_l$ is a coefficient smaller than a unity, shows almost the same result. For the resonance it was supposed in [4] that $m\iota = n$, then replacing $n$ through $m\iota$ makes two formulas very similar.

If the orbit stochastization takes place, it is possible to estimate the collisionless diffusion induced by the resonance interaction of the particles with the wave. The time needed for the particle to move away from the resonance surface on a distance of a half island width is

$$t^* \simeq \frac{\sqrt{r}}{2\pi} \left( \frac{\delta B}{B} \frac{R}{a} \cdot m\iota' \right)^{-1/2} .$$

Substituting typical stellarator reactor parameters and taking $\delta B/B$ of the order $10^{-4}$ yield the characteristic times of about $7/\sqrt{m}$ transit times for the resonance radius $r = 0.5$. That means that the particle makes a full period around the island in time $T \simeq 4\,t^*$, which is roughly one order of magnitude longer than the transit time. The diffusion coefficient can be constructed now as following:

$$D = \gamma \frac{(\delta r)^2 a^2}{(2\pi R/v)\, t^*} \simeq \left( \frac{R}{a} \frac{\delta B}{B} \right)^{3/2} \frac{v}{R} \frac{a^2}{r^{3/2}} \frac{\gamma}{\sqrt{m\iota'}},$$

where $\gamma$ is the fraction of the resonance particles. This expression gives very great values for the diffusion of the resonance particles, $D > \gamma \cdot 10^2\ m^2/s$, in the plasma regions where the orbits are stochastic.

Finally, we make a correction to formula (13) taking into consideration that not only the shear, but also the radial dependence of the drift velocity $v_d$ influences the island width. Returning to the expression for the mode phase (11), it is seen that the derivative of the rotational transform $\iota'$ over the dimensionless radius should be replaced in (13) by the combination $\iota' - (v_d/r)'\,(v_\parallel R/a)$. As a rule, the derivative in the second term here is negative, so, the poloidal drift can both increase and decrease the island width dependent on the $\iota$ radial profile.

## 8 Summary

A Hamiltonian guiding center code is applied to study single particle orbits in stellarators (Helias reactor and Wendelstein-7AS). The influence on these orbits of the time-dependent perturbations of the magnetic field produced by the global Alfvén

eigenmodes is investigated. Fourier representation of the plasma magnetic field and model or calculated plasma electric field were used.

It was found that the resonant interaction between the passing particles and the wave leads to the formation of the island-like structures on the drift surfaces. The amplitude of the perturbation sufficient to create such islands is in the range of $\delta B/B \simeq 10^{-5} - 10^{-4}$.

It was demonstrated elsewhere [11] that the finite plasma beta improves the confinement of the thermonuclear alphas in a Helias reactor. Our orbit calculations confirm this result. Diamagnetic effect produces non-zero radial gradient $\nabla_r B$, which in turn gives rise to a poloidal drift. This drift closes initially poloidally and toroidally blocked orbits deeply trapped in the main well (s. Sec. 3 and Fig. 2). The drift caused by the radial electric field plays a similar role. The resulting effect depends on the mutual orientation of the both drifts. The non-resonant magnetic fluctuations of the amplitudes $\delta B/B \simeq 10^{-4}$ do not affect substantially these orbits. It should be mentioned that the $\nabla B$-drift can be inverted by the inverting of the current in the field coils, whereas the $\mathbf{E}\times\mathbf{B}$-drift cannot. This fact gives a possibility to shift some of the resonances from the plasma.

The mode numbers of the perturbations, which resonate with the passing orbits were calculated. They depend on the relation between the Alfvén velocity $v_A$ and the particle velocity $v$. If $v_A > v$, then the resonances occur only in the vicinity of the "resonant" values of the rotational transform $\iota_s = n/m$. If $v_A < v$, the passing particle can resonantly interact with the broader range of the modes through the poloidal component of its drift motion. Co– and counter-going particles can now resonate with different modes.

Alfvén-like perturbations modifying the orbits can cause immediate particle losses if the island is located near the plasma edge and its width is large enough to intersect the plasma boundary. The particles located near the passing-trapped boundary can be pushed by the resonance fluctuations over it and become superbanana.

Under some circumstances the resonance condition can be fulfilled for two different modes at the same radial position. In this case the resonant particle interacts with these modes simultaneously, since the islands overlap even by small perturba-

tion amplitudes. After superposing of such two single resonant perturbations the island structure exists no longer. The result depends on the relative phase shift between the perturbations.

The threshold of the stochasticity onset in the resonance particle motion is dependent on the particle pitch and seems to be above the perturbation amplitude of $\delta B/B \sim 10^{-4}$ for the majority of the passing particles. Non-resonant passing orbits are weakly influenced by the perturbations of the amplitudes considered. Because of that, the criterion of the islands radial overlapping in configurational space is not sufficient for the orbit stochastization. It should be supplemented by the requirement on the value of the magnetic moment $\tilde{\mu}$, which must enable this particle to interact resonantly with the both perturbations.

The magnetic field shear plays an important role in the arising of the island structures. The radial size of the islands is larger in the systems with low $\iota'$. However, by the experimentally observed perturbation amplitudes and experimentally realized $\iota$-profiles they are smaller than the plasma radius. Hence, the anomalous losses can be caused mainly by the resonance overlapping and following orbit stochastization. On the other hand, in the low-shear stellarators, unlike tokamaks the number of the island chains in the plasma is smaller, what prevents in many cases their resonance interaction. Moreover, if $v_A > v$, as for W-7AS, avoiding of the magnetic islands in the plasma leads to disappearing of almost all drift surface islands as well.

The resonance interaction between the particles and the waves is sensitive to the plasma electric field and profile of the rotational transform. Thus, the detailed analysis of the orbits resonance behaviour in W-7AS and of the energetic particle losses as well can be carried out on the basis of knowing of these plasma characteristics.

It was found a formula for the island width coinciding with that obtained earlier [4]. The particle needs typically more than ten transit times to close its orbit around the island. This period can be used as a time step to estimate the coefficient of the collisionless diffusion of the stochastic orbits.

## Acknowledgments

We would like to thank Arthur Weller for the helpful discussions and Henning

Maaßberg, whose calculations of the plasma electric field were used in our model concerning W-7AS.

## References

[1] K.L Wong, et al. Phys. Rev. Letters **66**, 1874 (1991)

[2] W. Heidbrink, et al. Nucl. Fusion **31**, 1635 (1991)

[3] A. Weller et al. 34-th APS Annual Meeting, Seattle, 16–20.11.1992

[4] H.E. Mynick. Princeton Plasma Physics Laboratory Report, PPPL–2856, 1992

[5] D.J. Sigmar, C.T. Hsu. Phys. Fluids B **4** (6), 1506 (1992)

[6] R.J. Littlejohn. Phys. Fluids **24**, 1730 (1981)

[7] J. D. Meiss, R. D. Hazeltine. Phys. Fluids B **2** (11), 2563 (1990)

[8] R. B. White, et. al. Phys. Fluids **26**, 2958 (1983)

[9] J. Kißlinger. (Private communication)

[10] J. Geiger. (Private communication)

[11] W. Lotz, et al. Pl. Phys. and Contr. Fusion **34**, 1037 (1992).

[12] D.V. Sivukhin. In "Reviews of Pl. Phys." (ed. by M.A. Leontovich), V. **1**, Consultants Bureau, New York, 1965

[13] A. Weller. Discussions on "FIRE" Mode, June 24, 1992, IPP

## Figure captions

Fig. 1. Normalized Fourier components of the magnetic field strength.
a) Helias reactor [9]; b) Wendelstein-7AS.

Fig. 2. Isoline plots of $\mid B \mid$ on a single flux surface for a Helias reactor:
a) full set of Fourier harmonics [9]; b) model used for the orbit calculations.

Fig. 3. Isoline plots of $\mid B \mid$ on a single flux surface for the stellarator Wendelstein-7AS:
a) VMEC results [10]; b) model used in our calculations of the particle orbits.

Fig. 4. The illustration of a resonance between a passing particle with the parallel velocity $v_{\parallel}$ drifting poloidally with the velocity $u_d$ and a wave with the mode numbers $m$, $n < 0$. $u_{ph}$ is the phase velocity of the wave.

Fig. 5. The solution of the approximate equation (8) for the resonance conditions alpha particle-wave (Helias reactor). The point on the curve with the coordinates $(\tilde{\mu},\ r/a)$ denotes the particle orbit resonating with the mode $m$, $n$, whose values correspond to this curve.
a) counter-going orbits, b) co-going orbits.

Fig. 6. Poincaré plots (a-c) and an orbit projection on the plane $\varphi = const$ (d) of the 3.5 MeV counter-passing alpha particle in the Helias reactor. Particle magnetic moment $\tilde{\mu} = 0.84$, radial starting point $r/a = 0.65$, mode numbers $(m,\ n) = (-2, -1)$.
The perturbation amplitudes a) $\delta B/B = 10^{-4}$; b) $\delta B/B = 2 \cdot 10^{-4}$; c-d) $\delta B/B = 5 \cdot 10^{-4}$;

Fig. 7. Profiles of the rotational transform a) and of the Alfvén velocity (arbitrary units) b) in the Helias reactor.

Fig. 8. Resonance a) and non-resonance b) interaction between the passing particle and the wave. The particle parameters differs only in the sign of $v_{\parallel}$.
The perturbation amplitudes: a) $\delta B/B = 5 \cdot 10^{-5}$; b) $\delta B/B = 2.5 \cdot 10^{-3}$.

Fig. 9. Coupling of two resonances (co-going alpha particle with $\tilde{\mu} = 0.7$) located

radially close to each other: a) perturbation $(m,\ n) = (-2, -3)$, $\delta B/B = 2 \cdot 10^{-4}$;
b) perturbation $(m,\ n) = (-3, -4)$, $\delta B/B = 10^{-4}$;
c) the both perturbations simultaneously. The island structure is destroyed.

Fig. 10. Resonance curves for the interaction of 45 keV protons and Alfvén perturbation in W-7AS ($B = 2.5T$). Solid curves – co-going particles; dashed curves – counter-going particles. ($\iota$-profiles are taken from Ref. 12)
a) $\iota = 0.345 - 0.405$; $v_A(0)/v_p = 1.45$.
b) $\iota = 0.345 - 0.382$; $v_A(0)/v_p = 1.55$.
c) High $\iota$ case: $\iota = 0.50 - 0.58$; $v_A(0)/v_p = 1.81$.

Fig. 11. Resonance curves for the interaction of 45 keV protons and Alfvén perturbation in W-7AS ($B = 1.25T$). Solid curves – co-going particles; dashed curves – counter-going particles. ($\iota$-profiles are taken from Ref. 12)
a) Low $\iota$ case: $\iota = 0.27 - 0.283$; $v_A(0)/v_p = 1.06$.
b) High $\iota$ case: $\iota = 0.52 - 0.60$; $v_A(0)/v_p = 1.06$.
c) High $\iota$ case: $\iota = 0.51 - 0.57$; $v_A(0)/v_p = 1.22$.

Fig. 12. The 45 keV proton resonance orbits in W-7AS.
a) Co-going particle with $\tilde{\mu} = 0.5$, $(m,\ n) = (-5, -2)$, $\delta B/B = 10^{-4}$.
b) Counter-going orbit with $\tilde{\mu} = 0.5$, $(m,\ n) = (-3, -1)$, $r/a = 0.6$, $\delta B/B = 2 \cdot 10^{-4}$.
c) The previous case, but $r/a = 0.77$.

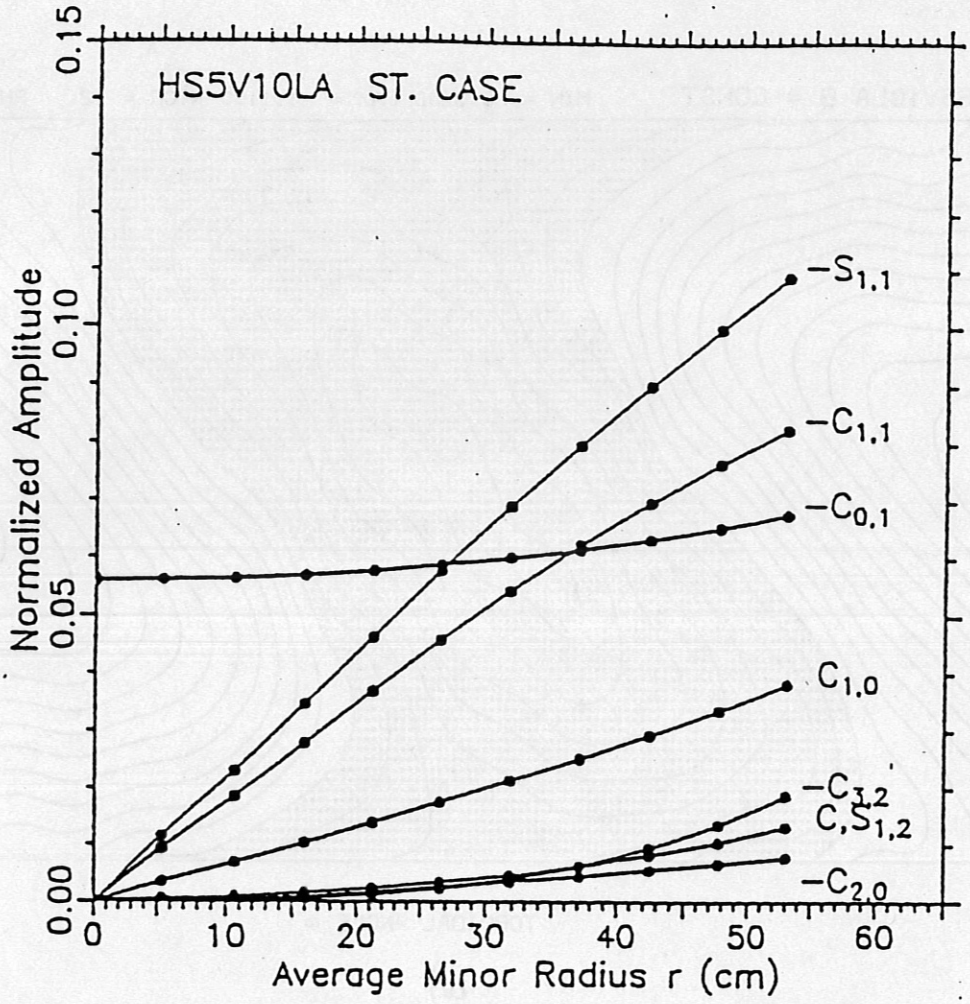
HS5V10LA ST. CASE
Normalized Amplitude
0.15
0.10
0.05
0.00
0
10
20
30
40
50
60
Average Minor Radius r (cm)
$-S_{1,1}$
$-C_{1,1}$
$-C_{0,1}$
$C_{1,0}$
$-C_{3,2}$
$C,S_{1,2}$
$-C_{2,0}$

a)

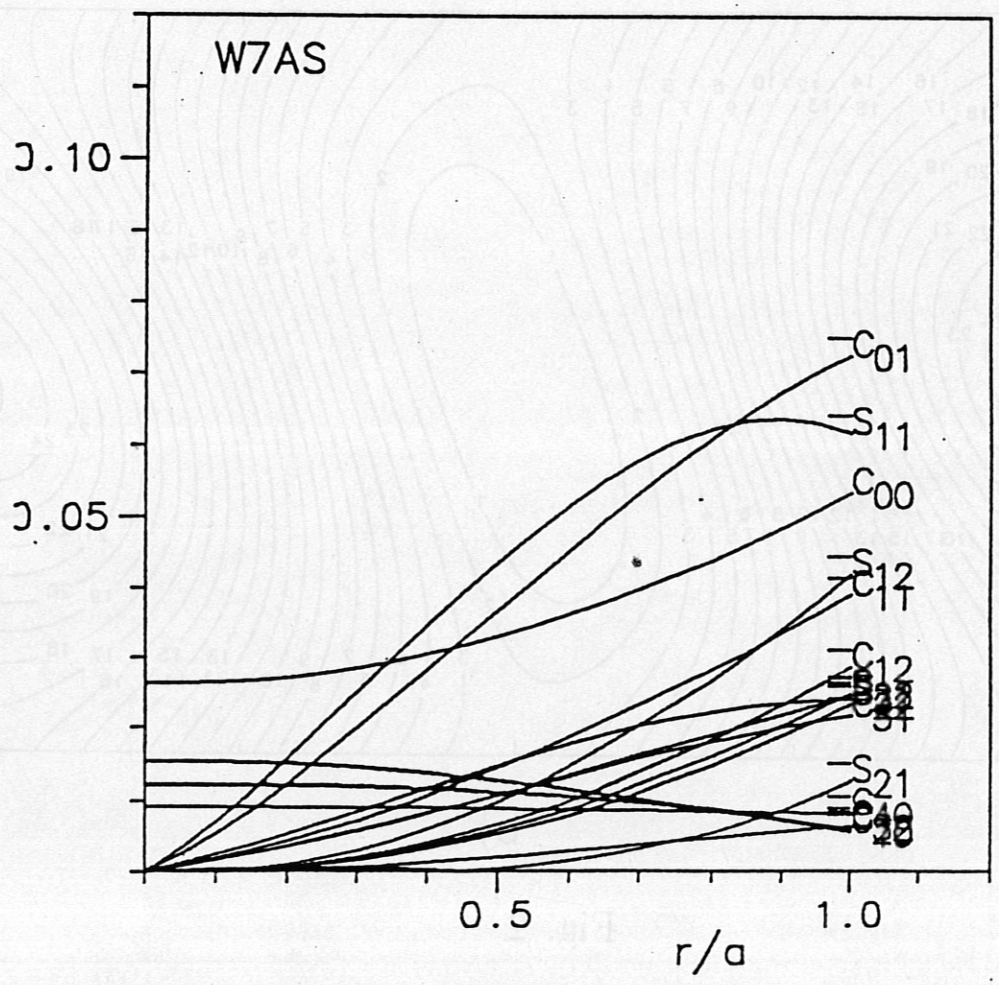
W7AS
0.10
0.05
0.5
1.0
r/a
$-C_{01}$
$-S_{11}$
$C_{00}$
$-S_{12}$
$-C_{11}$
$-C_{12}$
$-S_{21}$

b)

Fig. 1

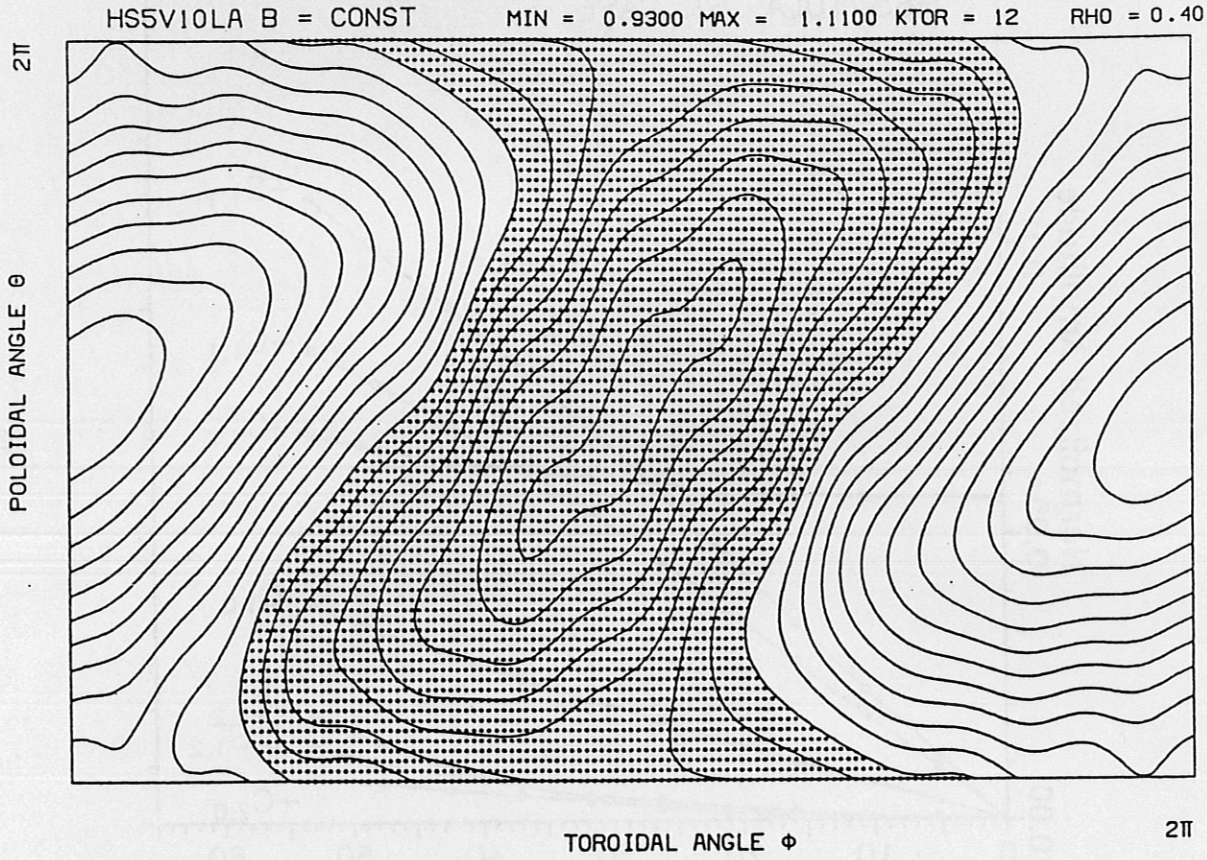
HS5V10LA B = CONST
MIN = 0.9300 MAX = 1.1100 KTOR = 12
RHO = 0.40
2π
POLOIDAL ANGLE θ
TOROIDAL ANGLE Φ
2π

a)

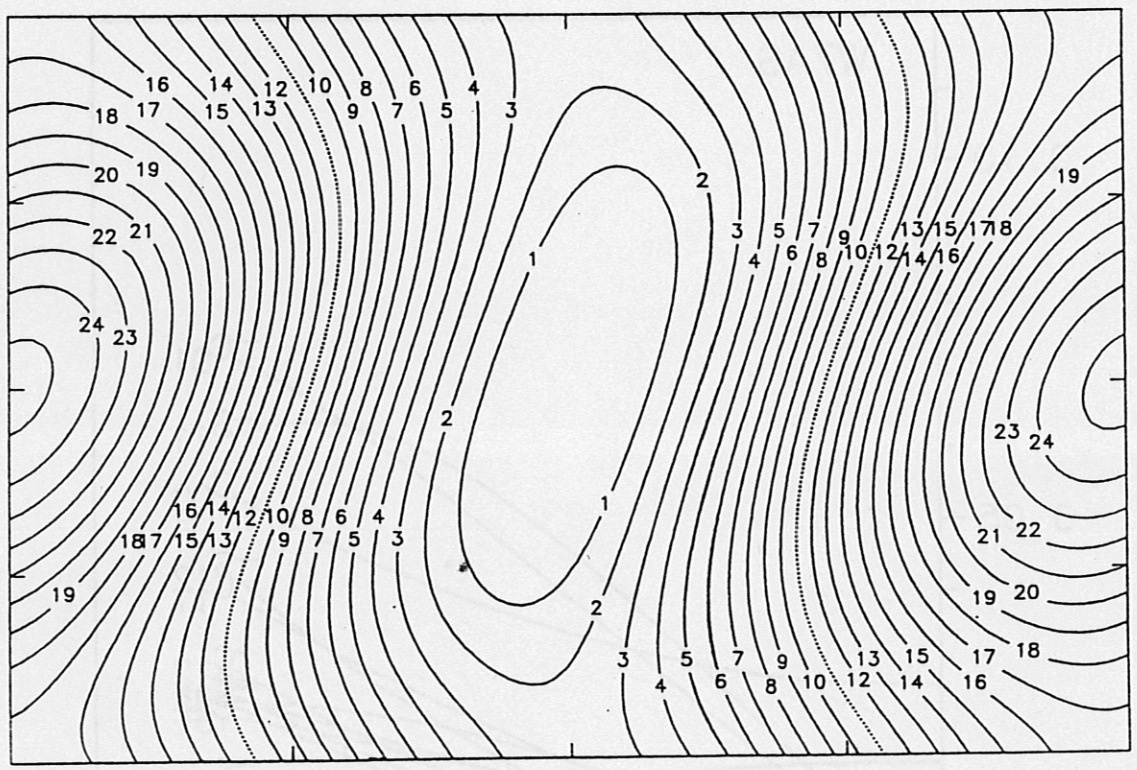

b)

Fig. 2

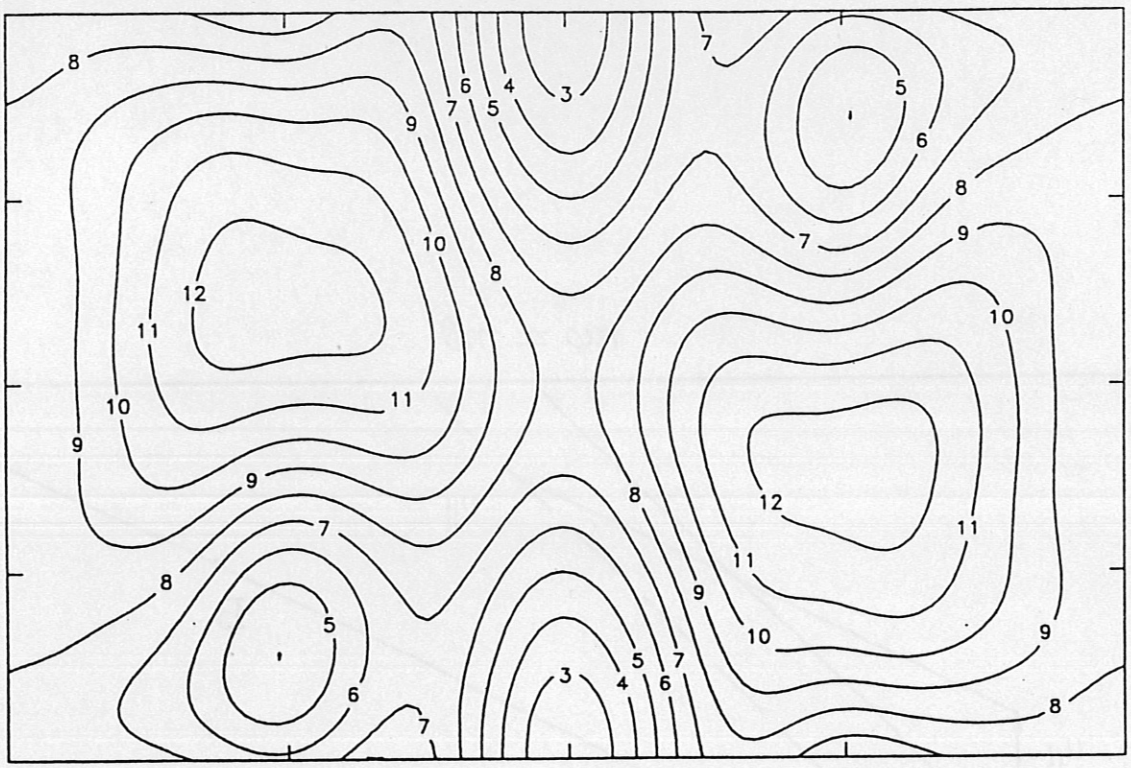
8
9
10
11
12
11
10
9
8
7
6
5
4
3
5
6
7
8
9
10
11
12
11
10
9
8
7
6
5
4
3
5
6
7
8
9
10
11
12
11
10
9
8
7
6
5
4
3
5
6
7
8
9
10
11
12
11
10
9
8
7
6
5
4
3

a)

b)

Fig. 3

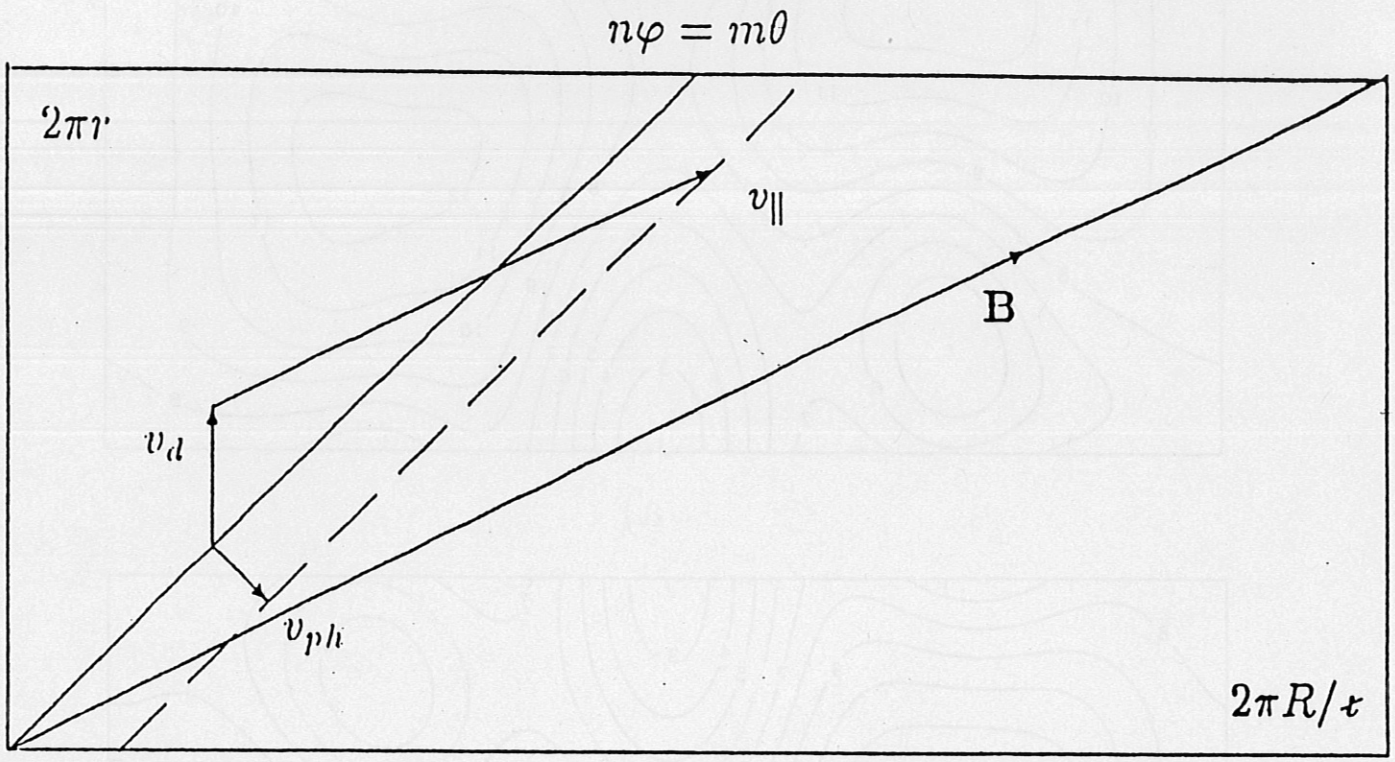


Fig. 4

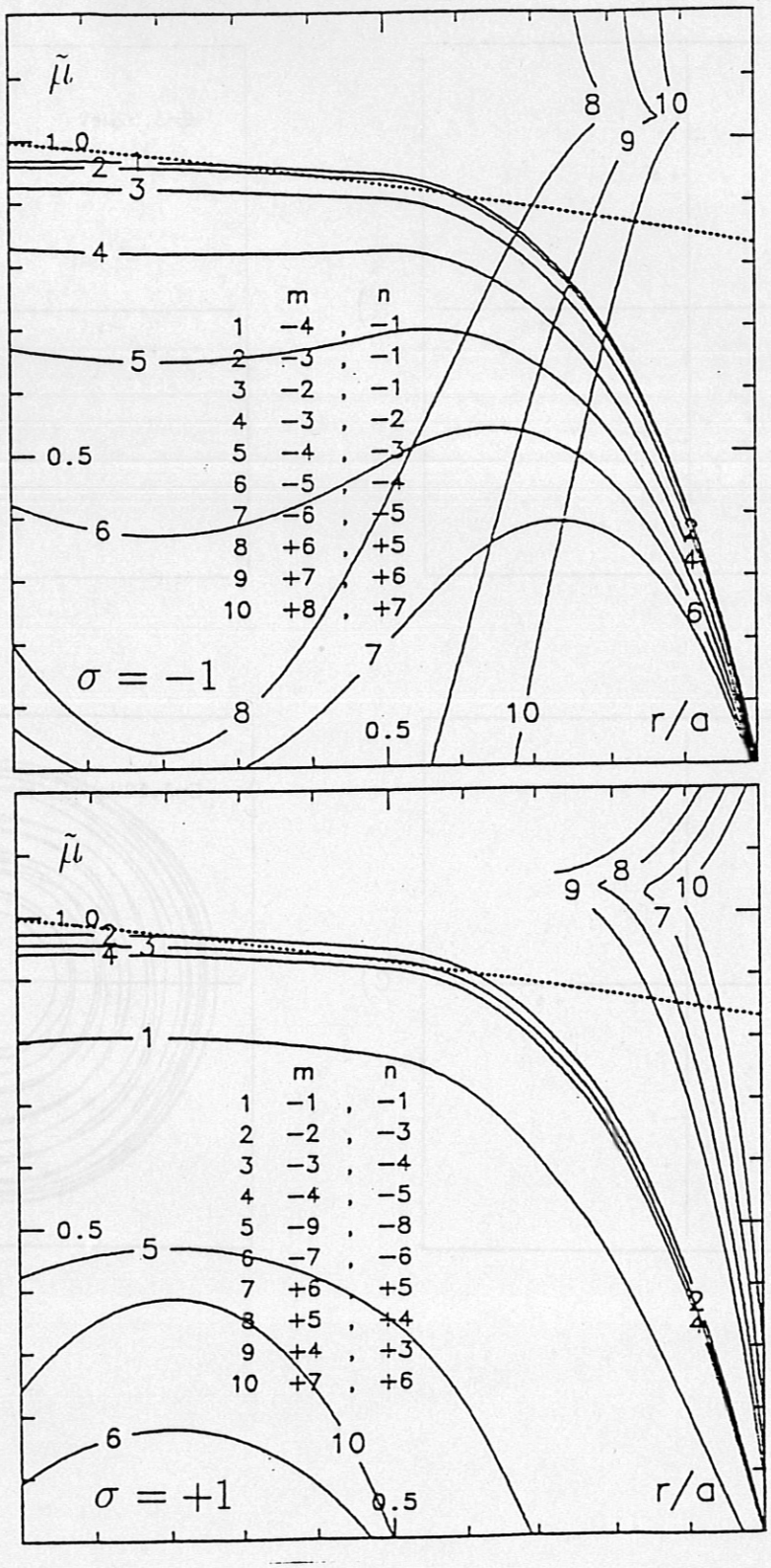
$\tilde{\mu}$
m n
1 −4 , −1
2 −3 , −1
3 −2 , −1
4 −3 , −2
5 −4 , −3
6 −5 , −4
7 −6 , −5
8 +6 , +5
9 +7 , +6
10 +8 , +7
$\sigma = -1$
r/a
0.5
$\tilde{\mu}$
m n
1 −1 , −1
2 −2 , −3
3 −3 , −4
4 −4 , −5
5 −9 , −8
6 −7 , −6
7 +6 +5
8 +5 , +4
9 +4 , +3
10 +7 , +6
$\sigma = +1$
r/a
0.5

a)

b)

Fig. 5

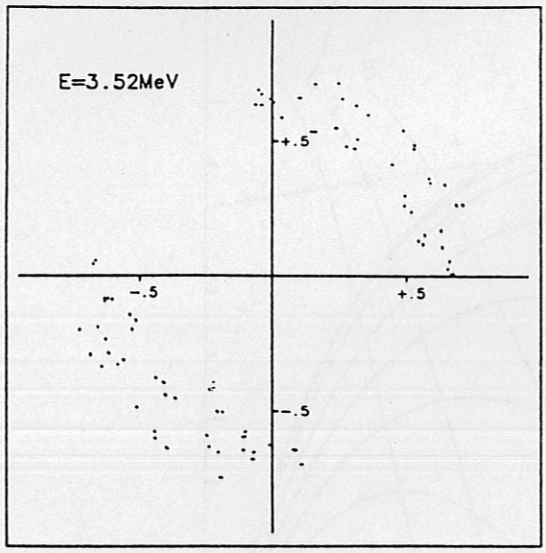


a)

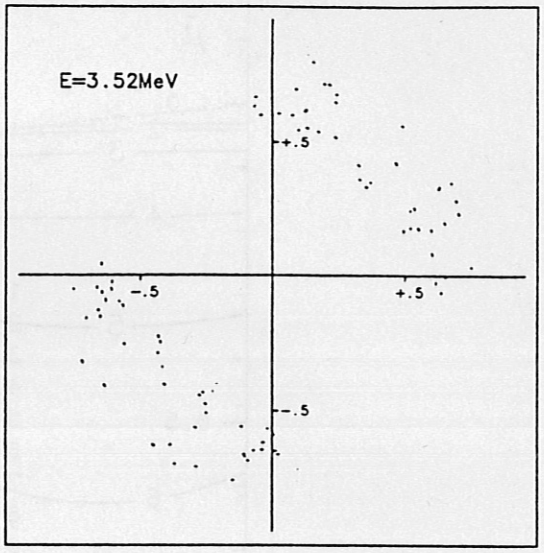


b)

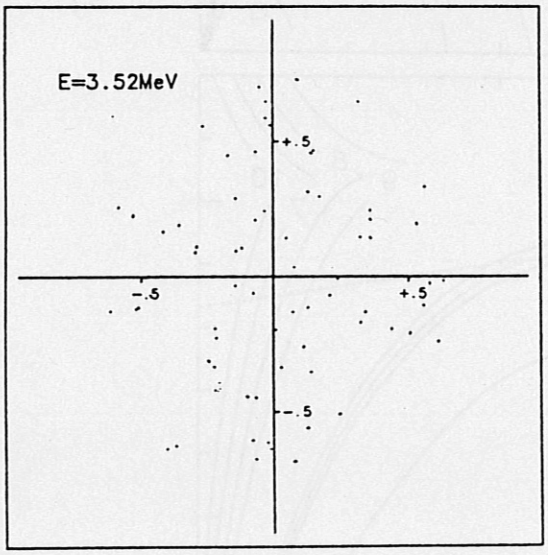


c)

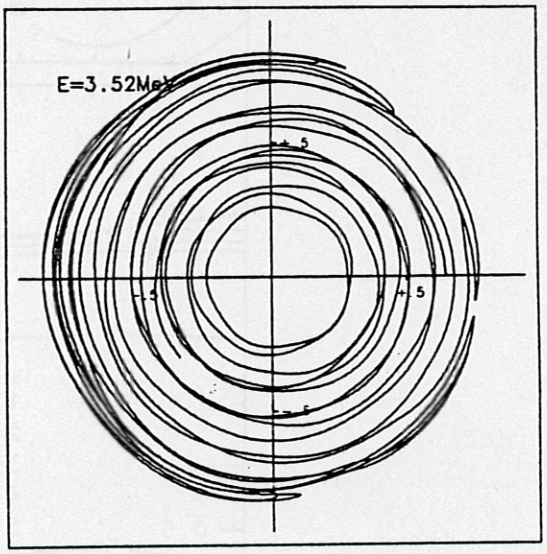


d)

Fig. 6

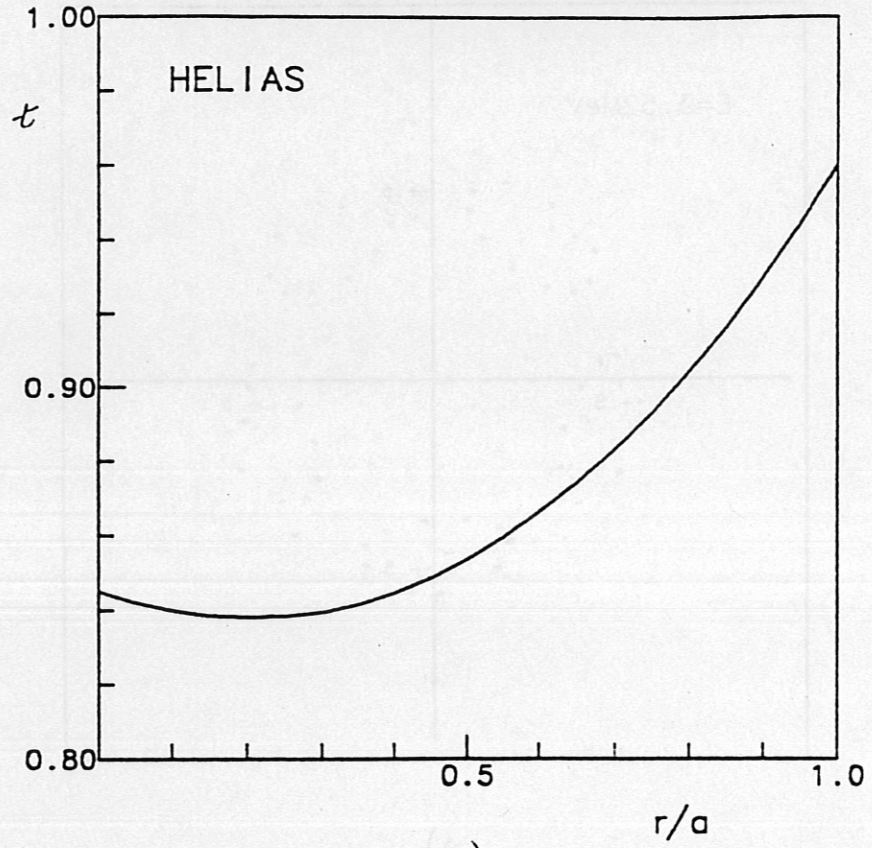


a)

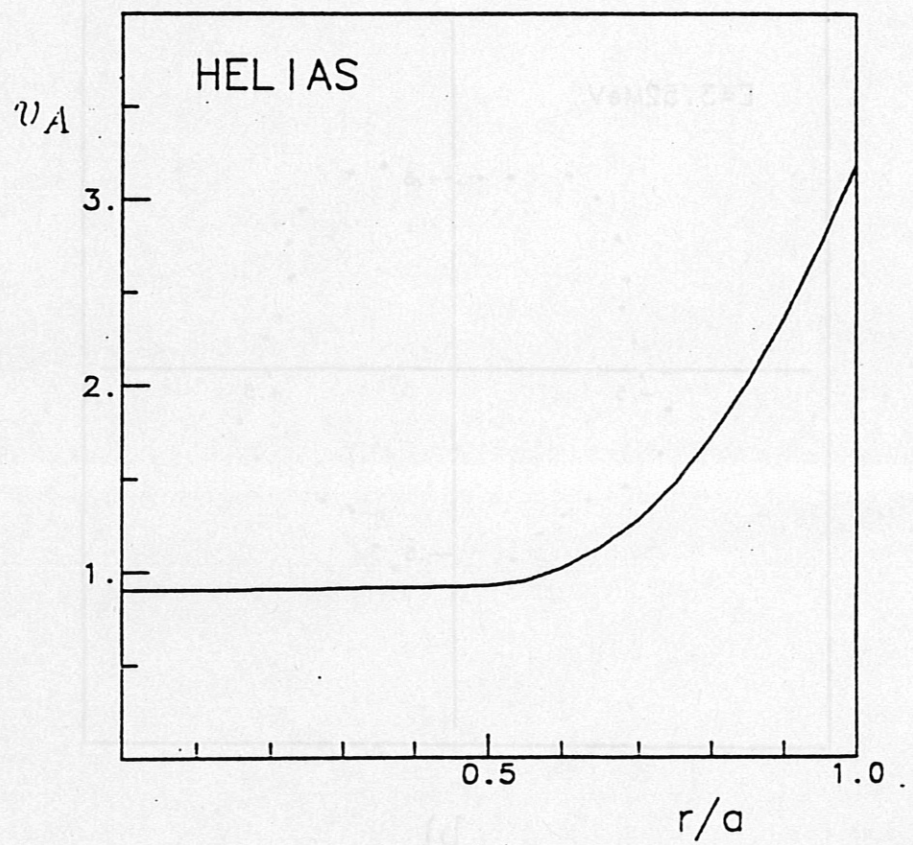


b)

Fig. 7

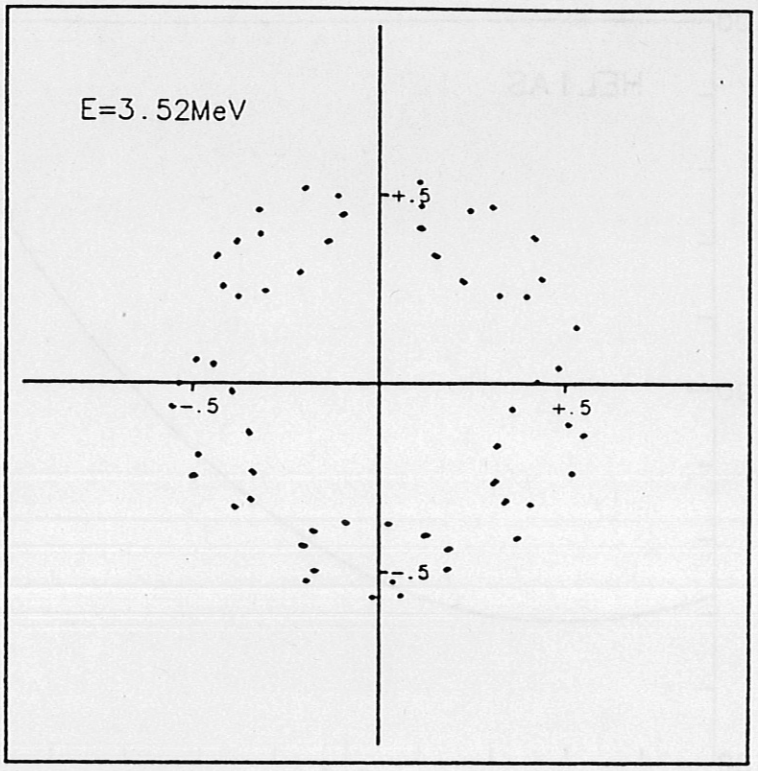


a)

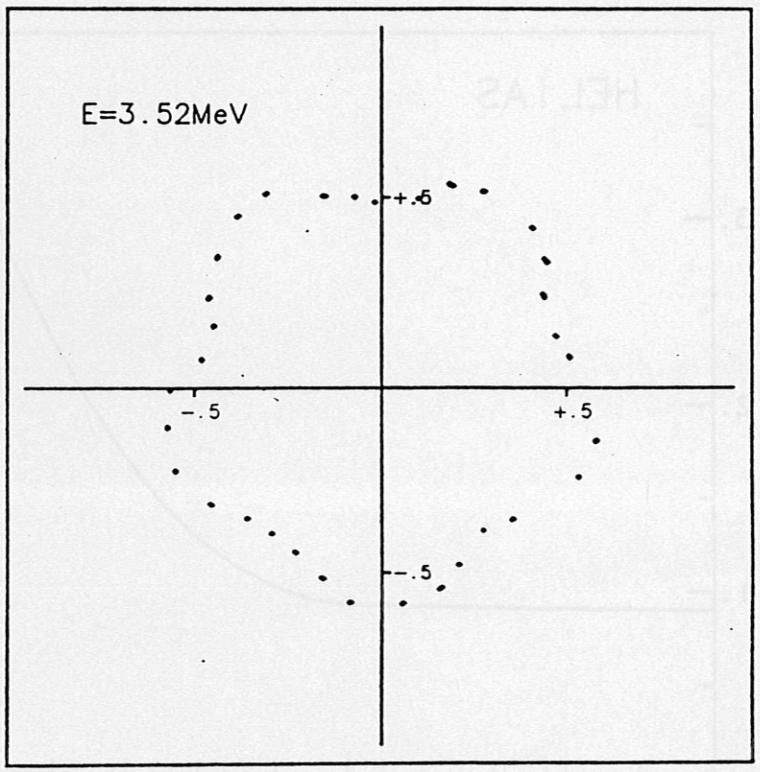


b)

Fig. 8

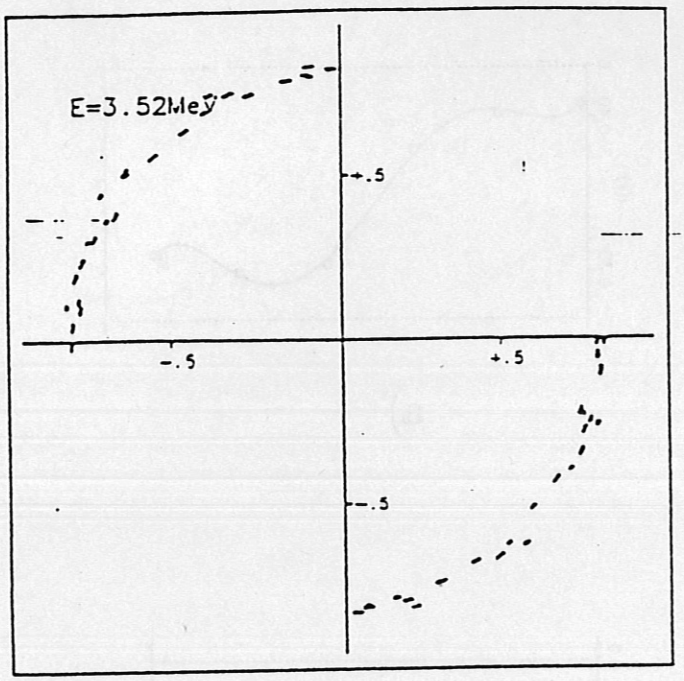


a)

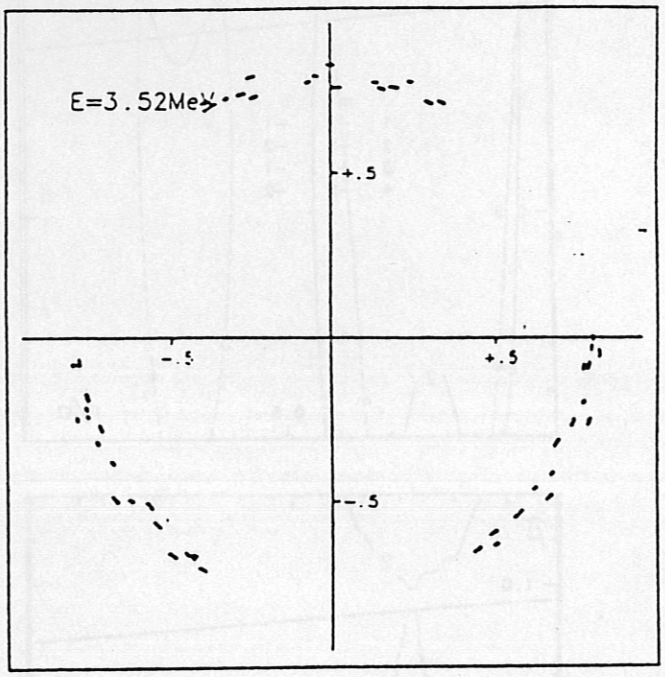


b)

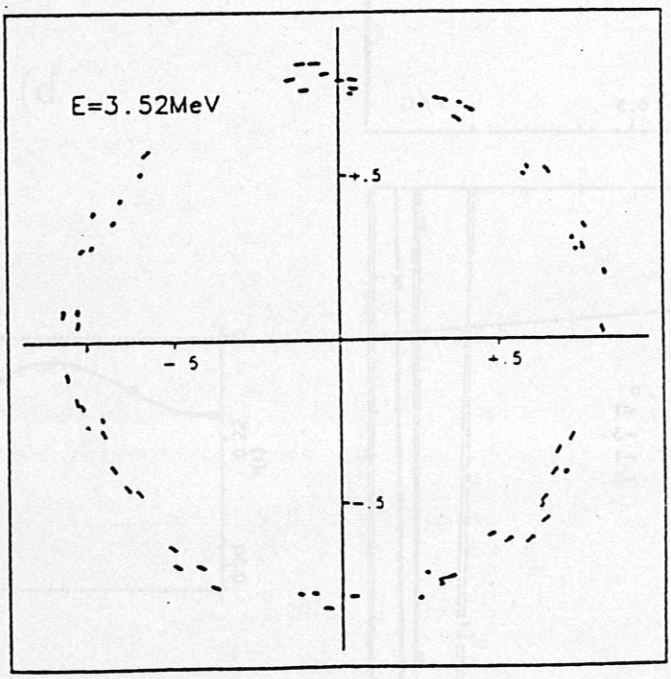


c)

Fig. 9

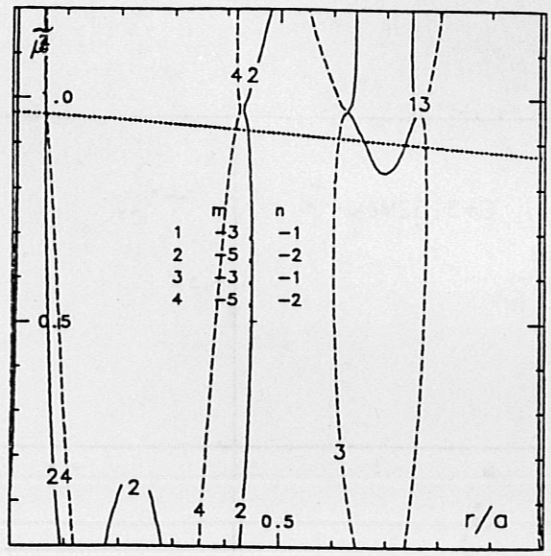
$\tilde{\mu}$
1.0
0.5
m
n
1 +3 -1
2 +5 -2
3 +3 -1
4 +5 -2
0.5
r/a

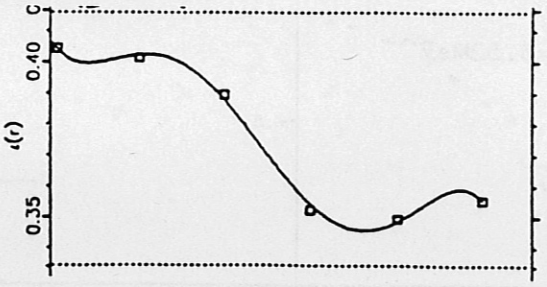
ι(r)
0.40
0.35

a)

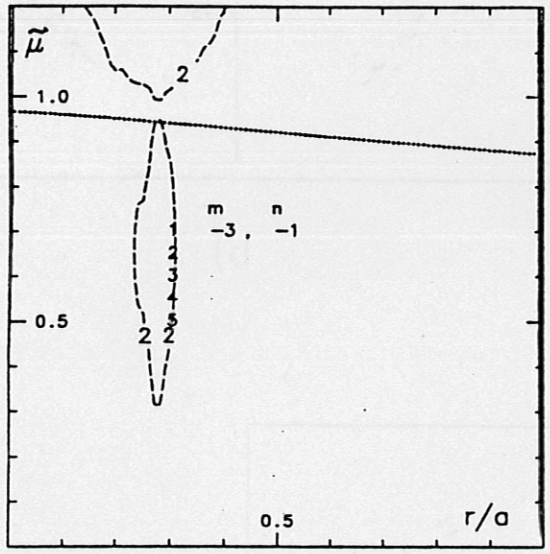
$\tilde{\mu}$
1.0
0.5
m
n
-3 , -1
0.5
r/a

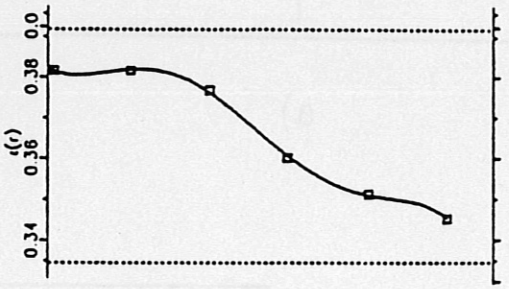
ι(r)
0.38
0.36
0.34

b)

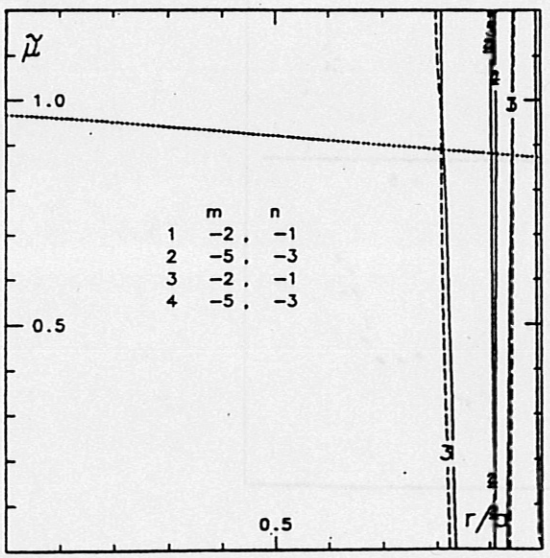
$\tilde{\mu}$
1.0
0.5
m
n
1 -2 , -1
2 -5 , -3
3 -2 , -1
4 -5 , -3
0.5
r/a

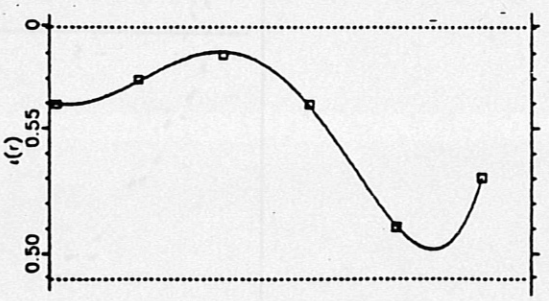
ι(r)
0.55
0.50

c)

Fig. 10

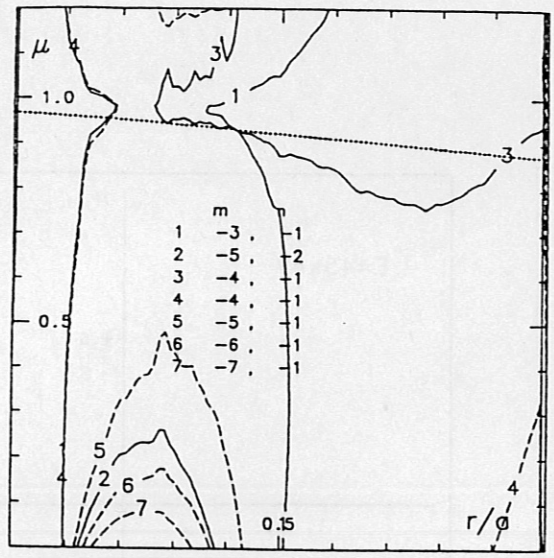
μ
1.0
0.5
m
1 -3 , 1
2 -5 , 2
3 -4 , 1
4 -4 , 1
5 -5 , 1
6 -6 , 1
7 -7 , 1
0.15
r/a

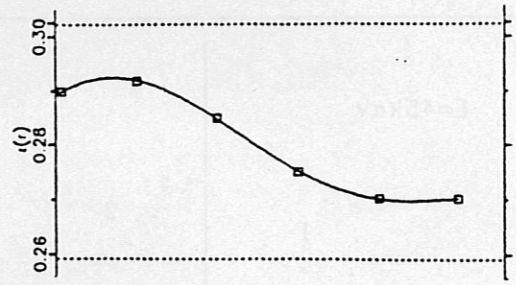
0.30
0.28
0.26
ι(r)

a)

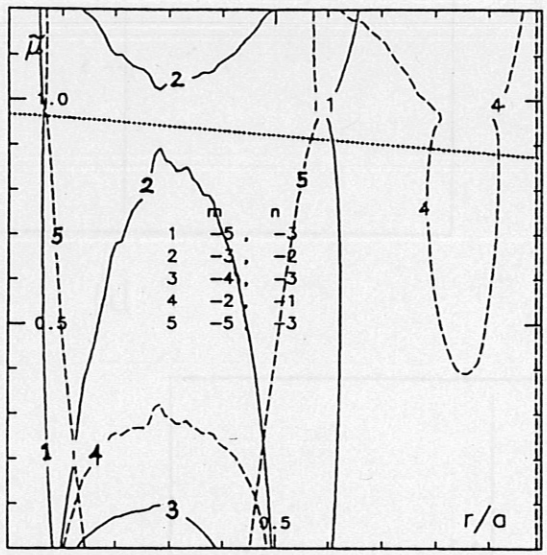
μ
1.0
0.5
m n
1 -5 , -3
2 -3 , -2
3 -4 , -3
4 -2 , -1
5 -5 , -3
0.5
r/a

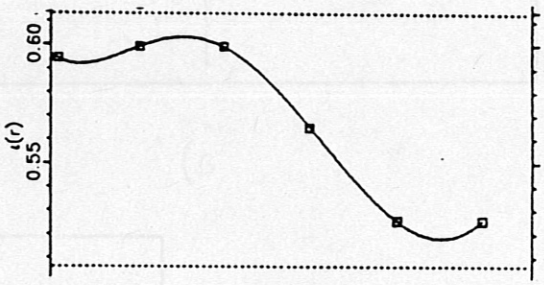
0.60
0.55
ι(r)

b)

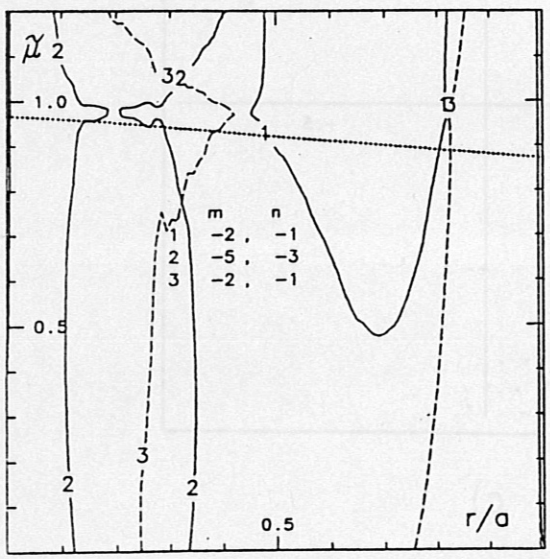
μ
1.0
0.5
m n
1 -2 , -1
2 -5 , -3
3 -2 , -1
0.5
r/a

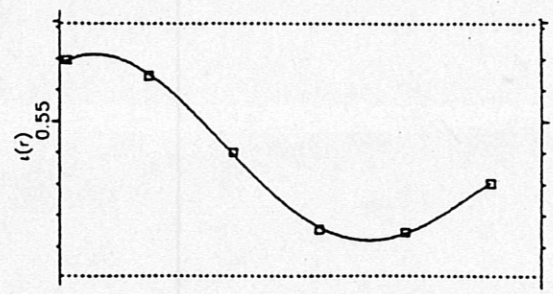
0.55
ι(r)

c)

Fig. 11

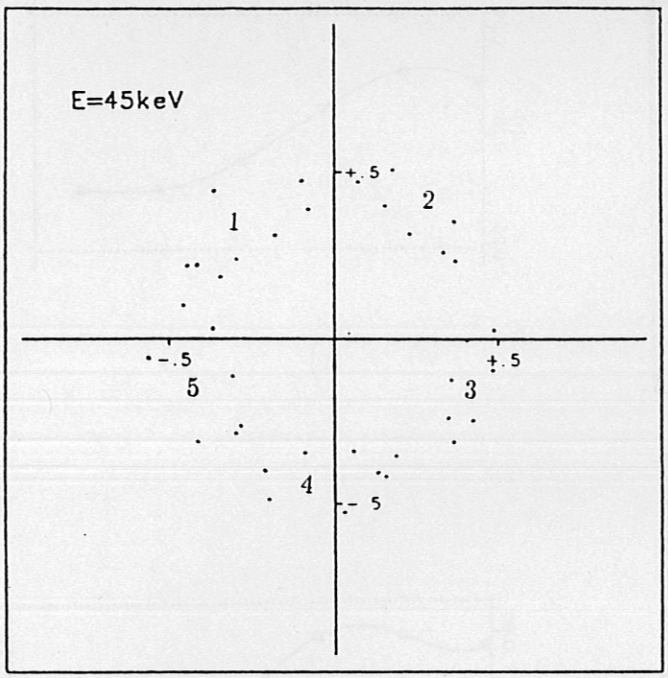


a)

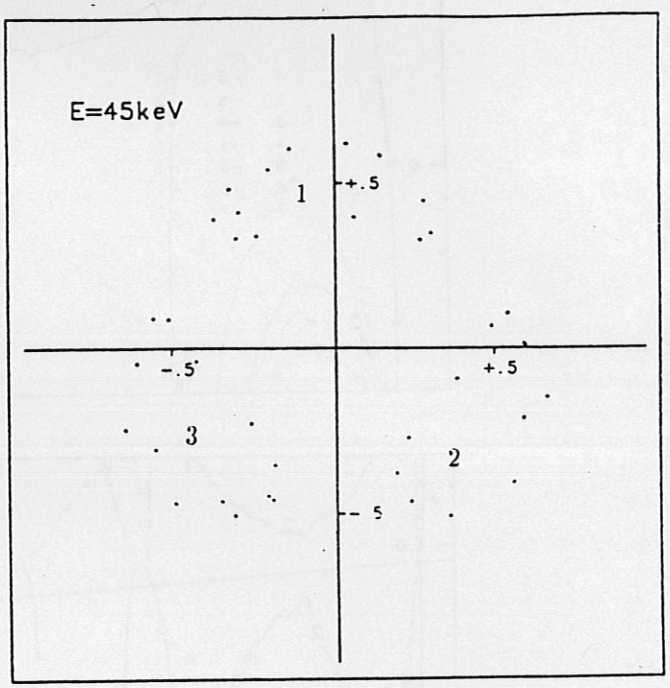


b)

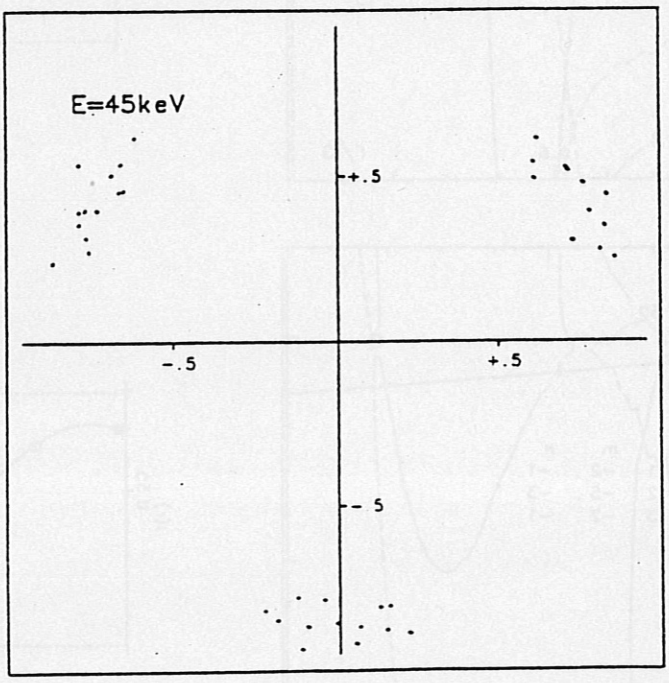


c)

Fig. 12